NTNU
Norwegian University of
Science and Technology

Numerical investigation of tip leakage vortex

Vegard Fredriksen

Master of Science in Mechanical Engineering
Submission date: June 2017
Supervisor: Michel Jose Cervantes, EPT

Norwegian University of Science and Technology
Department of Energy and Process Engineering

NTNU

Norwegian University
of Science and Technology

Department of Energy
and Process Engineering

EPT-M-2017-22

MASTER THESIS

for

Student Vegard Fredriksen

Spring 2017

Numerical investigation of tip leakage vortex

Numerisk analyse av tip leakage vortex

Background and objective

Tip leakage vortex (TLV) appears in many industrial applications, such as air transportation, space rockets and hydraulic machines. In the latter, cavitation may develop in the core of the TLV, often leading to severe erosion of the runner blades and the casing. The object of the project is to investigate numerically the TVL on a generic test case.
A literature review will be followed by numerical simulation to investigate the phenomenon in details. Special attention will be given to turbulence modelling, validation and mechanism.

The following tasks are to be considered:

1 Literature review: TVL, turbulence modelling
2 Determination of an appropriate test case for numerical investigation
3 Grid independency test
3 Turbulence model influence and validation
4 Mechanism behind TVL

-- ” --

Within 14 days of receiving the written text on the master thesis, the candidate shall submit a research plan for his project to the department.

When the thesis is evaluated, emphasis is put on processing of the results, and that they are presented in tabular and/or graphic form in a clear manner, and that they are analyzed carefully.

The thesis should be formulated as a research report with summary both in English and Norwegian, conclusion, literature references, table of contents etc. During the preparation of the text, the candidate should make an effort to produce a well-structured and easily readable report. In order to ease the evaluation of the thesis, it is important that the cross-references are correct. In the making of the report, strong emphasis should be placed on both a thorough discussion of the results and an orderly presentation.

The candidate is requested to initiate and keep close contact with his/her academic supervisor(s) throughout the working period. The candidate must follow the rules and regulations of NTNU as well as passive directions given by the Department of Energy and Process Engineering.

Risk assessment of the candidate's work shall be carried out according to the department's procedures. The risk assessment must be documented and included as part of the final report. Events related to the candidate's work adversely affecting the health, safety or security, must be documented and included as part of the final report. If the documentation on risk assessment represents a large number of pages, the full version is to be submitted electronically to the supervisor and an excerpt is included in the report.

Pursuant to "Regulations concerning the supplementary provisions to the technology study program/Master of Science" at NTNU §20, the Department reserves the permission to utilize all the results and data for teaching and research purposes as well as in future publications.

The final report is to be submitted digitally in DAIM. An executive summary of the thesis including title, student's name, supervisor's name, year, department name, and NTNU's logo and name, shall be submitted to the department as a separate pdf file. Based on an agreement with the supervisor, the final report and other material and documents may be given to the supervisor in digital format.

☐ Work to be done in lab (Water power lab, Fluids engineering lab, Thermal engineering lab)
☐ Field work

Department of Energy and Process Engineering, 15. January 2017

Michel Cervantes
Academic Supervisor

Research Advisor: Chirag Trivedi

PREFACE

This thesis is submitted as a part of the degree Master of Science in Mechanical Engineering at Norwegian University of Science and Technology (NTNU).

As a part of this study, a paper was written and presented at a hydropower conference in Nepal (the International Symposium on Current Research in Hydraulic Turbines (CRTH) - VII'17.).

I would like to thank my supervisor, Michel Cervantes, for providing good ideas throughout the semester. I will also like to thank my co-supervisor, Chirag Trivedi, for providing me with guidelines for English writing. And at last, I will thank my brother, Steinar, for proofreading this thesis.

Trondheim, June 11, 2017

Vegard Fredriksen

ABSTRACT

The Kaplan turbine has a small clearance gap between the blade tip and casing to allow the blades to rotate freely. This clearance gap is the cause of an undesirable Tip Leakage Vortex (TLV). A TLV might reduce the turbine efficiency, erode the turbine blades or cause instabilities for the power output.

A literature study indicated that the tip clearance gap was a critical parameter affecting the behavior of the TLV. A research gap was observed for an operating Kaplan turbine where the turbine shafts tend to wobble slightly, and thus fluctuate the tip clearance gap.

The aim of this thesis is to gain a better understanding of the Tip Leakage Vortex and investigate the research gap observing the effects generated by a fluctuating tip clearance gap.

To examine the effects, a numerical study was completed on a mesh of 7 million elements. The selected turbulence models were Shear stress transport (SST) and Scale-adaptive simulation (SAS).

The numerical results produced values close to the experimental results. Simulated results showed that the negative effects associated with TLV worsened when including the wobbling from the turbine shaft. For the smallest clearance gap, the maximum vortex strength showed an increase of 4 % compared to the maximum vortex strength of a stationary test. Tested on for stationary case, the radial forces showed a peak with a clearance gap size of 5 mm. The effects of a fluctuating clearance gap showed a significant increase of the maximum radial forces.

Obtained results show that further improvements are possible in the hydropower industry.

SAMMENDRAG

Kaplanturbinen har en liten klaring mellom turbinbladspissen og turbinhuset for at bladene skal kunne rotere fritt. Denne åpningen (klaringen) kan forårsake en uønsket lekkasje som genererer en virvelstrøm, på engelsk Tip Leakage Vortex (TLV). En TLV kan redusere turbineffektiviteten, erodere turbinblader og skape ustabilitet i kraftproduksjonen.

Det ble gjennomført et litteraturstudie som indikerte at størrelsen på klaringen mellom turbinbladspissen og turbinhuset er en kritisk parameter for hvordan en TLV oppfører seg. Litteraturstudie viste at for roterende Kaplanturbiner med slark i akslingen medfører at klaringen mellom bladene og turbinhuset varierer.

Målet med denne oppgaven er å få en bedre forståelse av Tip Leakage Vortex og undersøke effektene en varierende klaring har på en TLV.

For å undersøke effekten nærmere er numeriske simuleringer blitt gjennomført med et mesh på 7 millioner elementer. Turbulensmodeller ble valgt til Shear stress transport (SST) og Scale-adaptive simulation (SAS) for den numeriske modellen.

De numeriske resultatene ble sammenlignet med eksperimentelle referanseresultater, og de viste god overensstemmelse. De numeriske resultatene viste at de negative effektene som var forbundet med TLV, ble forverret når en inkluderte slark fra en turbinaksel. Ved den minste klaringen økte den maksimale virvelstyrken til TLV'en med 4% i forhold til det stasjonære tilfellet. Den radikale kraften hadde en betydelig økning ved en klaring på 5 mm. Ved en varierende klaring viste resultatene en betydelig økning for radial kraft i forhold til stasjonære tilfeller.

Oppnådde resultater viser at ytterligere forbedringer er mulige i vannkraftbransjen.

CONTENTS

NOMENCLATURE

Greek letters

α	Hydrofoil incidence angle	$[\circ]$
Γ	Circulation	$[m^2/s]$
Γ_c	Total circulation	$[m^2/s]$
ν	Kinematic viscosity	$[m^2/s]$
ρ	Density	$[kg/m^3]$
τ_{wall}	Wall shear stress	$[N/m^2]$
ω	Vorticity	$[m/s]$

Acronyms

CFD	Computational Fluid Dynmics
LES	Large Eddy Simulations
RANS	Reynold-Averaged Navier-Stokes
RMS	Root Mean Square
SAS	Scale Adaptive Simulations
SST	Shear Stress Transport
TLV	Tip Leakage Vortex

Roman letters

c	Chord length	$[m]$
P	Pressure	$[N/m^2]$
r_c	Vortex core radius	$[m]$
r	Radius	$[m]$
u_i	Velocity in x, y, z	$[m/s]$
$\overline{u_i}$	Time-averaged velocity	$[m/s]$
u_∞	Free stream velocity	$[m/s]$
v_r	Radial velocity	$[m/s]$
v_z	Axial velocity	$[m/s]$
v_θ	Tangential velocity	$[m/s]$

INTRODUCTION

1.1 INTRODUCTION

Hydropower is Norway's most important energy resource. In 2015 hydropower stood for 95.8 % of Norway's total electricity production [3]. On a world basis, hydropower stands for approximate 17 % of the world's electricity production [4]. As the world transfers towards renewable energy, and with limited water resources, the extraction of water energy should be optimized. Norway utilizes approximately 80 % (136.45 TWh) of its technologically and economically feasible water resource potential [5]. Only a slight increase of the overall turbine efficiency in Norway, like 0.01 %, is equivalent to a year's electricity consumption for almost 7000 Norwegian's households [3]. Hence, it is important to constant chase improvements in the hydropower industry.

To capture the water energy, a wide range of different turbines has been designed to optimize the efficiency and minimalize the downtime. Despite decades of development, some designs continue to have a potential for improvement. One of these, the Kaplan turbine, is subjected to downtime due to blade erosion and unpredictable efficiency losses from leakage flow. These are issues that the industry might is able to overcome or marginalize.

The Kaplan turbine, and other axial rotating machinery, need small clearance gap between the blade tip and casing to allow the blades to rotate freely. The generated pressure difference over the turbine blade drives, in the clearance gap, a leakage flow, which rolls over to an undesirable Tip Leakage Vortex (TLV). The TLV might reduce the turbine efficiency, erode the turbine blades or cause instabilities for the power output. For the Kaplan turbine, several aspects affect the leakage flow and TLV, such as the blade thickness, blade tip velocity, blade roughness and the tip clearance gap size. Additionally, for the latter, Kaplan turbine shafts tend to slightly wobble when it rotates, and thus diverse the tip clearance gap size.

The existence of the TLV phenomena is found in multiple industrial applications such as pumps, turbines, and aerospace, and hence has motivated scientists from many fields. Still, the flow physics behind the tip leakage vortex is not yet fully understood.

1.2 THESIS OBJECTIVE

The aim of this study is to gain a better understanding of Tip Leakage Vortex in Kaplan turbines. Potential research gaps within the field could be discovered by studying existing literature, and a literature review will be the framework for constructing an appropriate test case in this thesis. The test cases will be investigated through numerical simulations, which are both time and cost efficient method compared to experiments. Numerical results will be experimentally validated and discussed.

Furthermore, the literature review, later presented in Chapter 2, identified an existing research gap regarding the effects on the TLV from the clearance gap variations generated by the wobbling of the Kaplan turbine shaft. In this thesis, the identified researched gap will be examined closer and more in detail.

2 RESEARCH INSIGHT

In this chapter is previous work regarding the Tip Leakage Vortex evaluated. The presented literature review includes industrial research broader than the hydropower industry.

2.1 LITERATURE REVIEW

The Tip Leakage Vortex phenomena was observed in the early 1980s when Lakshminarayana [6, 7] carried out experiments observing a compressor wake, detecting the behavior of the Tip Leakage Vortex. Lakshminarayana found the turbulence to be largest in the leakage flow-mixing region. Focusing on tip leakage, Lakshminarayana observed in another paper [8] that the local lift coefficient is strongly related to the leakage flow velocity with a maximum intensity at 75 % of chord length.

In more recent years (2015), for his Ph.D., M. Dreyer [9] conducted experiments with 1235 distinct flow configurations, and the experiments are one of the most profound within the TLV research field. Dreyer focused on the size of the tip clearance gap, obtaining a clearance size range where the Tip Leakage Vortex was strongest and thus should be avoided. Similarly, observing effects from different tip clearance gap sizes has been studied by experiment for pumps and turbines by Wu et al [10], Miorini [11], and simulated by You et al. [12], Decaixa et al. [13], Higashi et al. [14], Zhao [15], and Lampart [16] providing a wide range of simulations and experimental data for different tip clearance gap size. Decaixa also investigated the simulation by using two different turbulence modeling approaches, namely LES and RANS. Decaixa [13] and Dreyer [9] had the same flow configuration setup and agreement with their simulated and experimental results. All above findings conclude that the tip clearance gap size is one of the most important parameters for determining the features of Tip Leakage Vortex. With the uniform agreement, at relatively small gap sizes the size of the vortex is increasing with increasing clearance gap size.

In a turbine, there is a relative motion between the blade tip and the wall casing (endwall). Most TLV studies [i.e. 10-16], have been performed without any motion between hydrofoil and endwall. Experiments by Muthanna [17] and Wang [18] indicates that wall casing motion does not affect the vortex features much. Nevertheless, the axial velocity in the vortex core center, there is a 44 % deviation due to the wall motion. As many critical features are relatively unaffected by the wall motion, it is worth mentioning that wall motion markedly shifts the vortex core location.

Design methods to mitigate the vortex strength includes, among others, wall casing treatment (grooves), anti-cavitation lip, blade tip rounding and blade-tip injection. Wall casing treatment, was experimentally researched by Dreyer [6], Ma [19] and numerically by Legras et al. [20] and Qiang et al. [21], obtaining a reduced tip leakage flow at modest to none penalty to the performance. Grooves oriented at $45°$ showed the greatest effects. Still, wall casing treatment has yet only notable results at relatively small clearance gap sizes. With the method, anti-cavitation lip, a small "wall" on the pressure side of the blade, has been tested by Dreyer [9] and Motycak [22], obtaining a result of shifting the vortex core without affecting the turbine efficiency. However, at the moment there are no guidelines for the design for an anti-cavitation lip.

Blade-tip rounding has been researched by Wu [10], Dreyer [9] and in a paper by Fredriksen [Appendix]. All with agreeing results that bigger tip-curvation reduced the corner vortices and increasing the tip leakage flow, hence also increasing the vortex strength. The overall impact of the effects of the tip corner vortices is yet not fully explored.

Blade-tip injection was described and simulated by Li et al. [23]. It is a way to create an arbitrary wall in the clearance gap. This method is also highly dependent on the tip clearance gap size, but also on strength and position of the injection holes. Most of the research in this area has used air as a medium, this includes a doctoral thesis by Behr [24]. So far, studies in this area have achieved promising results, reducing and blocking the tip leakage flow. In Li's air case, tip injection was able to increase efficiency by $0.35\ \%$ points [23], while Behr draws uncertainties to the eventual losses coupled to some newly created secondary vortices.

The Kaplan turbine is one of many industrial applications where tip leakage vortices appear. A study on a model Kaplan turbine by Mulu et al. [25] and Cervantes et.al [26] provided useful data on the magnitude of the clearance gap size in an actual turbine model. In this Porjus U9 model test, the clearance gap size was set to $0 - 3\ mm$ [19] for a runner blade diameter of $0.5\ m$ [27], giving a gap size below $0.6\ \%$ of the diameter, whereas Dreyer's experiment ranged from $1.5 - 15\ \%$ of hydrofoil diameter. Mulu [25] and Cervantes [28] also mentioned that the clearance gap was varying due to the wobbling of the turbine. Empirical data obtained from Cervantes [28] indicates that the tip clearance gap size may differ up to $10\ \%$ of the mean size.

As many sources agreed on [9, 10, 13, 14], tip clearance gap size is of great importance for understanding the TLV. While the clearance gap variations generated from the wobbling of the Kaplan turbine shaft is an area not well investigated.

3 THEORY

In this Chapter will the TLV problem briefly be explained, and basic theory necessary for evaluating the problem, will be presented.

3.1 TIP LEAKAGE VORTEX IN KAPLAN MACHINERY

Flow over an asymmetrically curved or angled blade creates pressure difference. In turbines, this pressure difference drives the turbine to rotate. The small gap needed in axial rotating machinery provides a passage for a pressure-driven leakage. This leakage flow rolls over to a vortex, Figure 1, referred to as Tip Leakage Vortex (TLV).

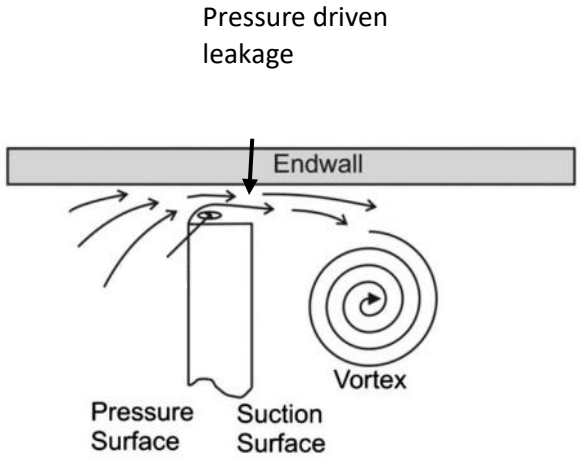

Figure 1. Tip leakage flow roll up to a tip leakage vortex [2]

In the Tip Leakage Vortex core, there is a pressure drop that sometimes leads to cavitation. Cavitation is an undesirable effect and could cause erosion on the turbine blades and the turbine casing. The magnitude of the pressure drop is highly depended on the vortex strength, which can be evaluated in the form of circulation. Circulation is a scalar describing the global rotation of a fluid, with relation to the local rotation of a fluid element, vorticity (curl of the velocity), described in equation 3 by Stokes theorem:

$$\Gamma = \int \int_S \omega \cdot d\boldsymbol{S} \tag{1}$$

Where Γ is the circulation, ω is the vorticity, and S is a surface.

Obtaining the integration surface can be done through the radius of the vortex core. The vortex core radius, r_c, is in the simplest models defined as the area where the vortex behaves as a rigid body, where the tangential velocity is linearly proportional to the radius. In the outer region, $r > rc$, the behavior is irrotational, and the tangential velocity is inverse proportional to the radius. In some vortex models, like the Lamb-Oseen vortex model (see 3.2 Vortex theory), r_c is defined as the location with maximum tangential velocity.

3.2 VORTEX MODEL

There are no equations that could mathematically represent an exact behavior of a vortex [29]. Thus assumptions and simplification are used. In this thesis, the Lamb-Oseen vortex model is applied due to its simplicity.

Lamb-Oseen Vortex

Starting from the Navier-Stokes (N-S) equation in cylinder coordinates (Appendix), the Lamb-Oseen model [29] assumes for a vortex that $v_r = v_z = 0$, where v_r is radial velocity and v_θ is the tangential velocity. And the N-S equation reduces to:

$$\frac{v_\theta^2}{r} = \frac{1}{\rho}\frac{\partial p}{\partial r}$$
$$\frac{\partial v_\theta}{\partial t} = v\left(\frac{\partial^2 v_\theta}{\partial r^2} + \frac{1}{r}\frac{\partial v_\theta}{\partial r} - \frac{v_\theta}{r^2}\right) \quad (2)$$

Where p, ρ, t, r, ν are respectively pressure, density, time, radius and kinematic viscosity.

The Lamb-Oseen Vortex model solves equation 2 by assuming the initial condition $v_\theta(r, 0) = \frac{\Gamma}{2\pi r}$, where Γ is the circulation in m^2/s and can describe the vortex behavior, equation 3 [29].

$$v_\theta(r) = \frac{\Gamma}{2\pi r}\left(1 - \mathrm{e}^{-\frac{\mathrm{ar}^2}{r_c^2}}\right) \quad (3)$$

Where $a \approx 1{,}25643$ and $r_c < r < 2r_c$.

As equation 3 indicates, the circulation strength Γ is dependent on the radius r and the tangential velocity v_θ.

Further, it is possible to describe the circulation distribution to the radius by equation 4.

$$\frac{\Gamma}{\Gamma_c} = (1 - e^{-a \cdot \frac{r^2}{r_c^2}}) \tag{4}$$

Solving equation 4 shows that approximately 71 % of the total circulation lies within the vortex core, and about 99% of the total circulation lies within a disc with radius $2\ r_C$.

3.3 VORTEX DETECTION

The vortex could be detected multiple ways, like the pressure minimum in the vortex center, or methods based on the velocity gradient tensor like λ_2- and Q-criterions. The λ_2-criterion builds on the vortex generated pressure minimum by filtering out unsteady straining and viscosity pressure effects. The Q-criterion detect a vortex as where the magnitude of the vorticity is greater than strain rate magnitude [30]. The full mathematics behind these two criterions could be found in the Ansys User's Guide [31].

3.4 HORSESHOE VORTEX

As the flow close to the endwalls approach a hydrofoil's leading edge, it is created a local pressure gradient around the stagnation point. This local pressure gradient could make the endwall's boundary layers separate, which will, as seen in Figure 2, roll up to a so-called horseshoe vortex [32].

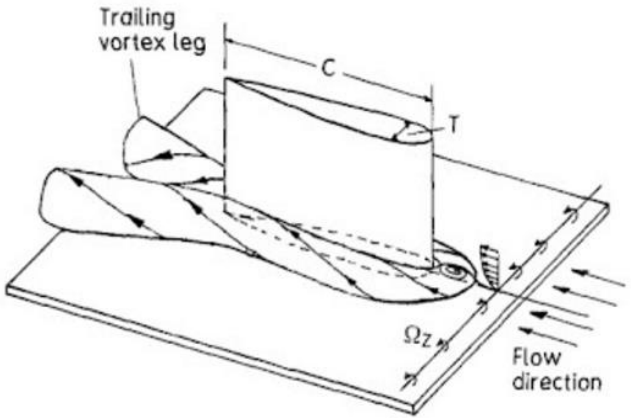

Figure 2. Horseshoe vortex: The boundary layer separates due to the high-pressure gradient around the stagnation point at the hydrofoil leading edge [1] .

The presence of the clearance gap will normally eliminate the endwall-hydrofoil stagnation point, and them rule out a horseshoe vortex. Nevertheless, Lampart [16] mentioned in his paper that the horseshoe vortex might occur if the clearance gap is tiny.

3.5 NUMERICAL APPROACH

A viscous flow can be continues described by the Navier-Stokes equation [33]:

$$\frac{\partial u_i}{\partial t} + u_j \frac{\partial u_i}{\partial x_j} = -\frac{1}{\rho}\frac{\partial P}{\partial x_i} + g_i + \nu \frac{\partial^2}{\partial x_i^2} \tag{5}$$

Where u_k is the velocity in the k^{th} direction, P is pressure, g is the gravity force, and ν is the kinetic viscosity.

Equation 5 is not analytical solvable for a complex flow. Numerical methods replace the continuous problem with a discrete gridded domain, referred to as meshing. The numerical solver used for this study (CFX), uses the discretization method, Finite volume method, which approximate the governor equations for each element. This approximation method is an iterative process, both solving non-linearity, and an extensive equation matrix. Different discretization schemes is a way to use the meshing point to linearize the governor equations. Most applications in CFX applies a High-resolution scheme [34], which is a blend between first order upwind and second order upwind to achieve a scheme that is fairly stable and accurate.

The iteration process continues until a given tolerance level, often when a convergence limit is reached. Some parameters to determine convergence of a solution is residual or variables of interest. *Residual* convergence often uses the parameter, Root Mean Square (RMS), which describes the global inequality in momentum-, continuity- and energy equation, where the observed variables are converged when they reach a steady state or a level of tolerance [35]. Variables of interest is converged when the monitored measuring points reach a degree of a steady solution.

3.6 TURBULENCE MODELLING

Turbulence is characterized as when the fluid's inertia forces are dominant over the viscous forces. This ratio is in fluid dynamics referred to as the Reynolds number (Re):

$$Re = \frac{uL}{\nu} = \frac{initial\ forces}{viscous\ forces} \tag{6}$$

Where $u,\ L, \nu$, is respectively velocity, length, and kinematic viscosity.

Turbulence (Re>4000 [33]) is as an unpredictable and random flow, defined by swirlings in the flow, and referred to as eddies. Turbulence models filter out and model the smallest time- and length-scale to create a numerical solvable flow. Without turbulence modeling, a full numerical resolution will require a grid with $Re^{9/4}$ number of nodes [36].

Reynolds-Average Navier-Stokes (RANS) is a modeling approach applying a time-average to the Navier-Stokes equation. RANS is not actually average over time, it is just a method to obtain the mean flow. Thus RANS is still time dependent. The RANS decomposing divides the flow into a mean and fluctuating variable, $u_i = \overline{u} + u'$. Applying the "time average" over the decomposed variables with the assumptions that a single fluctuation over time is zero, $\overline{u'} = 0$. RANS solves the mean flow, whereas the turbulence fluctuations have to be modeled. Time averaging the momentum equations (Equation 5) yields the Reynold Averaged Navier Stoke equation below:

$$\frac{\partial \overline{u_i}}{\partial t} + \overline{u_j}\frac{\partial \overline{u_i}}{\partial x_j} = -\frac{1}{\rho}\frac{\partial \overline{p}}{\partial x_i} + \nu\frac{\partial^2 \overline{u_i}}{\partial x_j \partial x_j} - \frac{\partial}{\partial x_j}(\overline{u_i' u_j'}) \tag{7}$$

Where the last term, $\tau_{ij} = -\overline{u_i' u_j'}$, referred to as the Reynolds stress, describes the turbulence effects on the mean flow. Modeling is needed to solve the term which includes 6 unknowns. Boussinesq suggested that the mean deformation rate was proportional with the stress tensor [37], which is a resemblance between turbulent and laminar flow. The proposed analogy simplified the Reynolds stress to only two unknowns, *turbulent kinetic energy*, κ, and *eddy dissipation*, ϵ [38].

The two-equation models use transport equations for the mean turbulent kinetic energy and turbulence dissipation, described as *eddy dissipation*, ϵ, and opposite, *specific dissipation*, ω. Menter [39] presented a turbulence model that blends the two models based on eddy- and specific dissipation referred to as the Shear Stress Transport (SST) turbulence model. The SST utilize the best parts of the modeling of ϵ and opposite ω, resulting in a less sensitive model. The SST turbulence model is a highly diffusive model, hence a robust model that will converge for most cases. In transient flow simulation, the SST could unintendedly catch the unsteadiness in the flow, and then struggle to converge. The setback of RANS models is that it mainly provide mean flow solutions, and loses to capture the unsteady eddies accurately.

Scale Adaptive Simulation-SST (SAS-SST) is the other turbulence model that will be applied for the transient simulations. The SAS-SST improves the RANS approach by adding a von Karman dynamic length scale to capture the turbulence unsteadiness. Karman's length scale, defined by velocity gradients, is much smaller than RANS's length scale determined by time-averaged velocity gradients. Thus, the von Karman length scale can detect unsteadiness. For efficient simulations, SAS-SST applies the RANS solution for the steady regions, whereas a length scale defined filtering (LES-like) approach is applied in for unsteady regions. Studies like Davidsen [40], a comparison of SST and SST-SAS, shows that the SAS term reduces the turbulent viscosity and thus the SAS-SST has an advantage resolving the turbulence fluctuations.

Wall treatment

The boundary layer's sub-region, viscous sublayer, is described by equation 8.

$$u^+ = y^+, \;\; 0 < y^+ < 11.6 \tag{8}$$

Within this region, the walls are treated through a wall function, equation 9-11 [34].

$$u^+ = \frac{U}{u_t}, \qquad y^+ = y\frac{u_t}{\nu} \tag{9}$$

$$u_t = \left(\frac{\tau_{wall}}{\rho}\right)^{0.5} \tag{10}$$

$$u^+ = 5.25 + 2.5 \cdot \ln(y^+) \tag{11}$$

Where U is the wall-parallel velocity, ρ is the density, τ_{wall} is the wall shear stress, and ν is the kinetic viscosity.

For a case with a varying clearance gap size, it is expected to develop detached eddies, eddies away from the walls, and the models are not bounded by having y^+ values around 1. A proper wall function could achieve satisfactory results but might fail to provoke the turbulence properly. Hence, a reasonable small y^+ value is desirable, but not a criterion. A resolved boundary layer is achieved with a y^+ value of around 1.

For the SST turbulence model, the Ansys CFX solver applies an automatic near wall treatment. Thus, it is not limited by which viscous layer the first mesh node lies within.

3.7 ERRORS AND UNCERTAINTIES IN NUMERICAL SIMULATIONS

There are many stages through a numerical process that could be subjected to error-generation. Errors could occur due to discretization, iteration, number round-off and physical modeling of turbulence and fluid assumptions. For a user to cope with the uncertainties in numerical simulations, experimental validation is necessary. A validation process will provide a scale on how accurately the simulations represent the real world

4 METHODOLOGY- SENSIBILITY ANALYSIS

This chapter describes the approach for choosing an appropriate simulation setup. Theory from Chapter 3 and test cases presented here will be the framework for the final setup. The Ansys' CFD software will be used for the numerical study. The geometries will be created in DesignModeler, meshed in ICEM and solved in CFX. A majority of the simulations are run on NTNU's supercomputer Vilje.

4.1 DOMAIN AND GEOMETRY

For validation purposes, the domain and geometry will match Dreyer's experiment [9]. The model used is an NACA0009 hydrofoil, originally 110 mm, here truncated at 100 mm, with a maximum height of $h = 10\ mm$. The blade-tip on pressure side is rounded with a 1mm radius. The hydrofoil is tilted at 7° to inlet flow direction. This will create the pressure differences that drives the leakage flow. Figure 3 shows the geometry setup and how the hydrofoil is placed in the tunnel where it is attached to the sidewall.

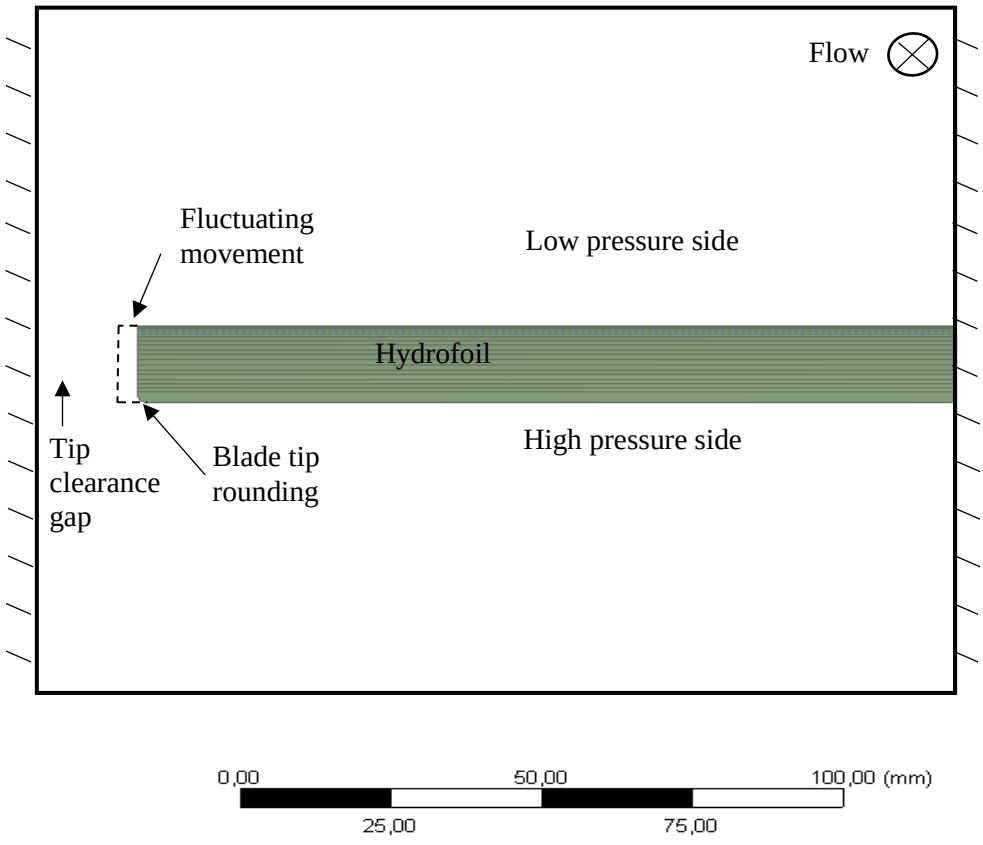

Figure 3. Flow domain including Hydrofoil observed in flow direction. [Ansys designModeler]

The outlet boundary conditions might affect the overall result on the flow domain. For optimal accuracy of the results, the outlet should be set as far away from the hydrofoil as possible, but this is not efficient due to computational time. Larger domain will lead to higher computational time. Thus, the optimal domain length will be evaluated between accuracy and available computational time.

For this case, to have a uniform velocity profile for the inlet, the computation domain for the simulation is only set to one chord length upstream the leading edge. A sensibility test is applied to obtain the length of the downstream domain. Four different tunnel lengths were tested. The drag force is a parameter that is depended on the downstream wake and chosen as a parameter of interest for this test. The test was done at steady state, with an SST turbulence model, and an inlet velocity of $10\ m/s$, an incidence angle at $7°$, and a tip clearance gap of $10\ mm$.

Figure 4 shows the normalized lift and drag values with the total domain length. The Figure indicates that the drag and lift reach a convergence for a domain with a total length of 10 chords. The shorter domains show some variance, especially for the drag value. A total length of 10 chord lengths seems to be a good tradeoff for computational time and accuracy, and further studies will use this length.

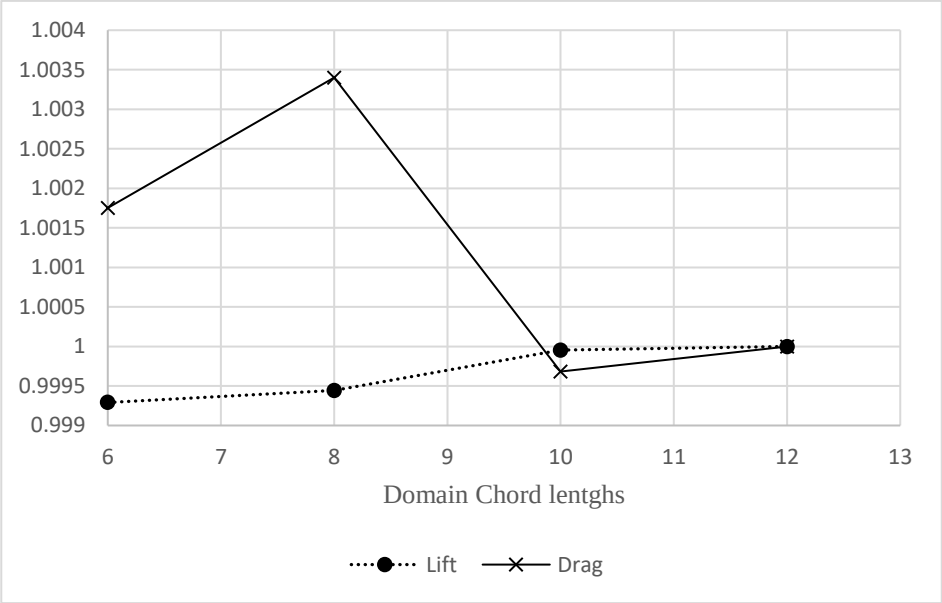

Figure 4. Evolution of drag and lift forces with the toral domain length, $\alpha = 7°$, $\tau = 1.0$, $W_\infty = 10m/s$.

4.2 MESH INDEPENDENCE STUDY

Ansys ICEM was used to create the mesh, allowing for full control for blocking and creating a structural hexahedral mesh. For evaluating the numerical convergence, three different mesh densities were tested at steady state with the SST turbulence model and a clearance gap size of 5 mm. Applying the procedure described by Celik [41] equation 13-16 yields the results shown in Table 1 (The whole table could be found in Appendix).

$$p = \frac{1}{\ln(r)} \left| \ln \left| \frac{\epsilon_{32}}{\epsilon_{21}} \right| \right| \tag{13}$$

Where $r = 1.3$, $\epsilon_{21} = \Phi_2 - \Phi_1$, Φ_k *is a parameter solution on* k^{th} *mesh*

$$\Phi_{ext}^{21} = \frac{r^p \Phi_1 - \Phi_2}{r^p - 1} \tag{14}$$

$$e_a^{21} = \left| \frac{\Phi_1 - \Phi_2}{\Phi_1} \right| \tag{15}$$

$$GCI_{fine}^{21} = \frac{1.25 e_a^{21}}{r^p - 1} \tag{16}$$

Where r is the mesh scaling factor

The three mesh sizes try to fulfill the same level of accuracy for the boundary layer to avoid switching between resolving the boundary layer region and CFX's automatic near wall treatment (Chapter 3.5).

Steady state simulations are applied to save time compared to transient simulations. The four parameters were chosen to fit the problem, where drag and lift indicate the quality of the mesh around the hydrofoil. Where the tangential velocity, v_θ, and Axial core velocity are critical values for post-processing results and are needed for validation. For axial core velocity, absolute values have been used, rather than using the deviation from free flow, W_∞, and the reader should assess that parameter accordingly.

Table 1. Four parameters, drag, lift, tangential velocity and axial core velocity are compared for three different mesh densities. The velocities are obtained 0.7 chord lengths behind the hydrofoil's trailing edge.

	$Parameter$	$Elements$ (Millions)	$Drag$ (N)	$Lift$ (N)	v_θ (m/s)	$Axial\ core\ velocity$ (m/s)
$Fine$	M_1	16.40	24.41	405.45	4.12	10.96
$Medium$	M_2	7.25	24.56	405.17	4.09	10.90
$Coarse$	M_3	3.61	25.01	404.25	3.94	10.71
	R_{21}	1.296	1.30	1.30	1.30	1.30
	P		4.32	4.61	5.73	4.79
	M_{ext}^{21}		24.34	405.57	4.13	10.98
	e_a^{21}		0.006	0.001	0.008	0.005
	e_{ext}^{21}		0.003	0.000	0.002	0.002
	GCI_{fine}^{21}		0.36 %	0.04 %	0.30 %	0.26 %
	GCI_{medium}^{32}		1.10 %	0.12 %	1.32 %	0.90 %

Presented in Table 1, the apparent order of the solution arrived at the range of 4.3-5.7. The small deviation between the fine and medium mesh indicates that the medium mesh has converged for all four parameters. Hence, for further simulations, the medium mesh was selected.

Mesh

Figure 5 shows the mesh structure around the curved hydrofoil. The displayed mesh is the one chosen from mesh independence study with 7.25 million elements. The domain stretched respectively one and eight chord lengths upstream and downstream. Focus area for meshing was to capture relevant areas that affect the flow, this includes hydrofoil boundary layer, vortex filaments, and cross flow, and thus these areas have a dense mesh. A primary purpose for the mesh is to capture the vortex behavior correct. From previous work, the location of the vortex was approximately known. A denser mesh was set over the vortex trajectory area, while rougher meshes were applied in areas with the expectation of small to none flow disturbances.

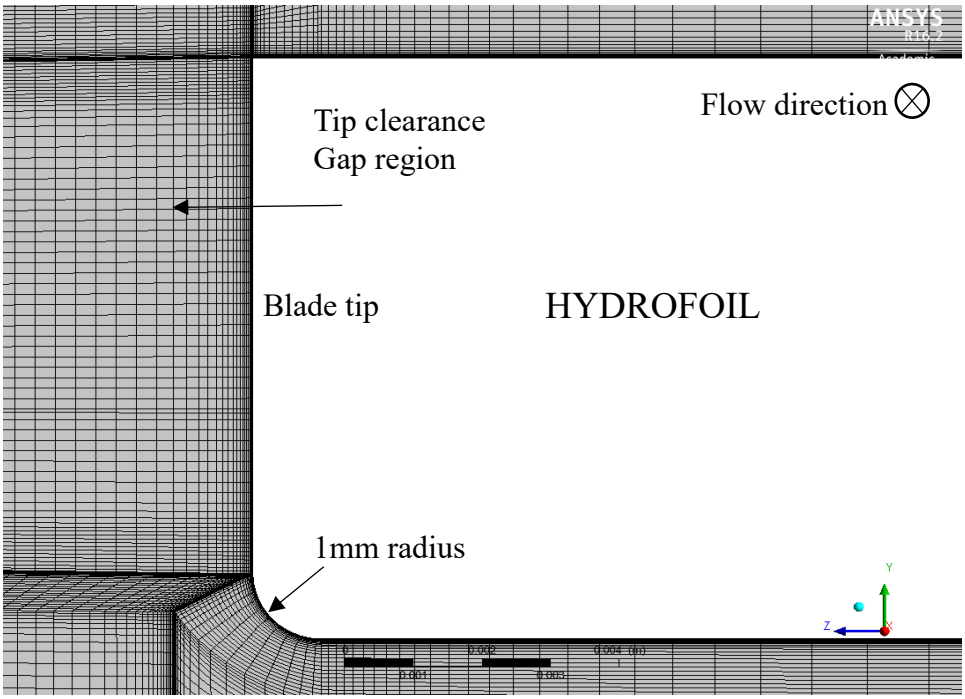

Figure 5. Sectional cut mid-hydrofoil, $0.5c$*, presenting the mesh around the rounded hydrofoil and a part of the clearance gap.*

By simulations, the y^+ values (Equation 9, Chapter 3.6) over the hydrofoil was obtained. These results showed an average of 4, whereas a max of 20, which is not sufficient to fully resolve the boundary layers. Thus, the wall function (Equation 11, chapter 3.6) is applied.

For the mesh deformation, the mesh stiffness is selected to increase near small volumes. Initial meshes were set for the maximum and minimum displacements (Chapter 4.5, Table 5) for the mesh deformation. The minimum angle of the elements for the clearance gap sizes at $10\ mm, 1\ mm\ and\ 0.3\ mm$ were $22.6°, 13.7°and\ 5.5°$ respectively. Tests ensured that the mesh retained the mesh quality under the deformation. The smaller gap sizes allowed for fewer elements in the clearance gap. Thus, the mesh sizes ranged from $6.5 - 7.25\ million$ elements.

4.3 FLUCTUATING CLEARANCE GAP

There are two possibilities for fluctuating the clearance gap size. Figure 4 (Chapter 4.1) shows the hydrofoil is attached to the wall on the right side. One possibility is to shrink the clearance gap by moving the left wall. The other way is to shrink the clearance gap by moving the right wall with the attached hydrofoil. The second option will best resemble the reality where the turbine shaft is fluctuating. This will include the shear stress on the hydrofoil surface, which is believed to play a part. It should also be noted that undesirable effects could appear due to the compression of the tunnel upstream and downstream the hydrofoil.

Data obtained from literature provides an indication on what tip clearance gap sizes that could be tested. A wide range of clearance gap sizes are applicable. Data from Dreyer [9], indicates that i.e. $1\,mm$ and $10\,mm$ are suitable candidates. Data collected from Kaplan turbine modeling [25, 26] suggests that a clearance gap size down to $0.3\,mm$ could be of interest. From information gathered by Cervantes [28], the fluctuating displacement will be set to $10\,\%$ of mean clearance gap size. The time-dependent variance of the clearance gap will follow a sine wave curve. The frequency for the clearance gap fluctuation is chosen to match a typical rotational speed of a model Kaplan turbine, where one rotation represents a fluctuation cycle. Data obtained from a Kaplan model test corresponded to a frequency of $10\,Hz$. The setup is shown in Table 2.

Table 2. The setup for the fluctuating clearance gap size

Test case	Mean Clearance gap size (mm)	Frequency (Hz)	Amplitude (% gap size)
1	10	10	10
2	1	10	10
3	0.3	10	10

4.4 TIME STEP STUDY

As CFX is an implicit solver, using backwards Euler, the simulation is unconditionally stable and in that sense independent on the Courant number [34]. Hence, the time step study focuses on the numerical accuracy, and the time step should be small enough for the solution to converge. The chosen mesh (7.25 million elements) from mesh independence study (Chapter 4.2) was used for the time stepping study. A transient simulation executed on a clearance gap of $1\ mm$, provided a vortex shredding frequency at the separation point just behind the hydrofoil, see Figure 6. The Fast Fourier transformation for this result, seen in Appendix, provided a vortex shedding frequency of $550\ Hz$. The separation point, seen in Figure 6, is a consequence of the truncation of the hydrofoil. It is expected that induced wall movement with a frequency of $10\ Hz$ dominates the flow, hence it is believed that the small flow separation will not play a vital part.

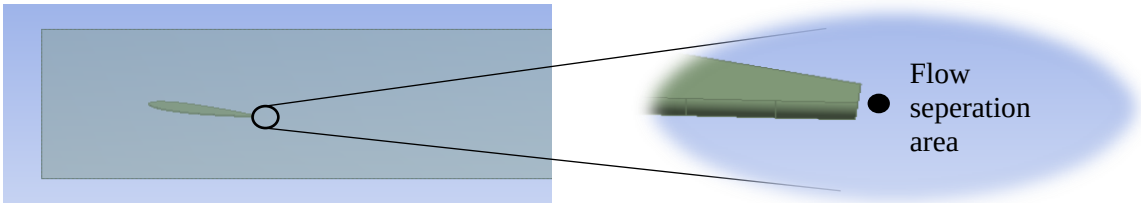

Figure 6. Separation point behind the hydrofoil [DesignModeler]

The time step set to capture the effects generated at $10\ Hz$ is set to the largest time step where the residual RMS reaches 10^{-4}, and the monitor points, defined by velocities and pressure, reach a smooth curve with a frequency of $10\ Hz$. The RMS convergence criteria are obtained from literature [35]. Transient simulations for a moving hydrofoil of $10\ Hz$ on a $5\ mm$ mean clearance gap indicated that a time step of $5 \cdot 10^{-4}\ s$ was sufficient to reach the RMS criteria. To capture the flow effects, typically at least 10 point per cycle ($10\ Hz$) should be evaluated. With a time step of $5 \cdot 10^{-4}\ s$, only approximately four points of the shredding cycle behind hydrofoil was obtained.

4.5 SETUP FOR THE SIMULATIONS

All walls were set to smooth with a no-slip condition. The inlet was set with a uniform velocity profile at $10\ m/s$ and the outlet with a reference pressure at $P_{ref} = 0$. The meshes applied are presented in chapter 4.2. The movement of the mesh was set to be stiffest at the small volumes. The setup for the simulation is given in Table 2 and 3.

Table 3. The numerical simulation setup

Domain setup

Fluid	Water
Tunnel dimensions	150x150 mm
Tunnel length	1 chord lengths in front
	8 chord lengths behind
Hydrofoil profile	NACA0009
Hydrofoil tip	Curved, 1mm pressure side
Incidence angle	7°
Turbulence model	SST, SAS-SST
Inlet velocity	10 m/s
Outlet	$P_{ref} = 0$
Walls	No slip wall

Table 4. The numerical simulation setup

Solver control

Advection scheme	High resolution
Transient scheme	Second order backward Euler
Turbulence numeric	First order
RMS	10^{-4}
Time step	$5 \cdot 10^{-4}$
Max coeff. loops	5
Precision	Double

The final results will first consist of eight simulations (4 SST, 4 SAS-SST) for validations. Then complete simulations with a fluctuating clearance gap size for three different mean clearance gap sizes. Next, getting the results for three more stationary hydrofoil simulations for comparisons. To observe the effects of the fluctuations itself a simulation is completed without any tip leakage flow, on the hydrofoil with an incidence angle of 0°.The table below is an overview of the simulations that will be presented in the result chapter.

Table 5. Overview of different simulation geometries

SST	SST-SAS	incidence angle $(degrees)$	Inlet/initial velocity (m/s)	
0.3mm	0.3mm	7	10	Stationary hydrofoil, maximum clearance gap size
1.0mm	1.0mm	7	10	
5.0mm	5.0mm	7	10	
-	0.29mm	7	10	Stationary hydrofoil, minimum clearance gap size
-	0.9mm	7	10	
-	11mm	7	10	
-	0.29-0.3mm	7	10	Moving hydrofoil
-	0.9-1mm	7	10	
-	10-11mm	7	10	
-	0.30-0.33mm	0	0	
-	0.9-1.0mm	0	0	
-	10-11mm	0	0	

5 RESULT AND DISCUSSION

This chapter investigates the accuracy of the numerical simulations through experimental validations. Some mechanisms around Tip Leakage Vortex are presented, and the effects due to a fluctuating clearance gap are observed. All results presented here are obtained from a flow over a hydrofoil tilted at $7°$ with an inlet and initial velocity of $10\ m/s$. The turbulence model selected is the SAS-SST. The measuring points was set downstream by 0.7 chord lengths, and the drag/lift/radial forces are measured at the hydrofoil.

5.1 VALIDATION

By comparing numerical simulations with experimental, one could magnify the error generated through the numerical process (Chapter 3.7). Experimental data is available for some part of this study. This makes it is possible to validate the simulations. Obtaining the vortex core center and the vortex core radius in the simulations is done by following Dreyer's experimental post-processing method.

The vortex core center is chosen as the place with the lowest pressure. According to the Lamb-Oseen vortex model, the vortex core radius was obtained where the average tangential velocity around the vortex core was at its maximum (Chapter 3.2). The area of the vortex core was applied as the surface (Equation 1, Chapter 3.1) for calculating the in-core vortex circulation.

Dreyer in his experiment has evaluated the circulation strength from a disc with radius $2\ r_c$ centered on the vortex. In the simulated results, the vortex core center was located relatively close to the endwall (flow domain boundary). In an attempt to apply Dreyer's method for the simulated result, a disc of radius $2\ r_C$, intersected with the endwall (flow domain boundary), which made this approach impractical. To overcome this issue, a disc with radius $1\ r_c$ remained within the flow domain. The obtained circulation had to be corrected with the Lamb-Oseen observation that only $71\ \%$ of the total circulation lies within a disc of radius $1\ r_c$.

Figure 7 presents the simulated and experimental dimensionless circulation results with respect to clearance gap size. The dimensionless circulation used for the validations is defined as:

$$\Gamma^* = \frac{\Gamma}{W_\infty \cdot r_c} \tag{16}$$

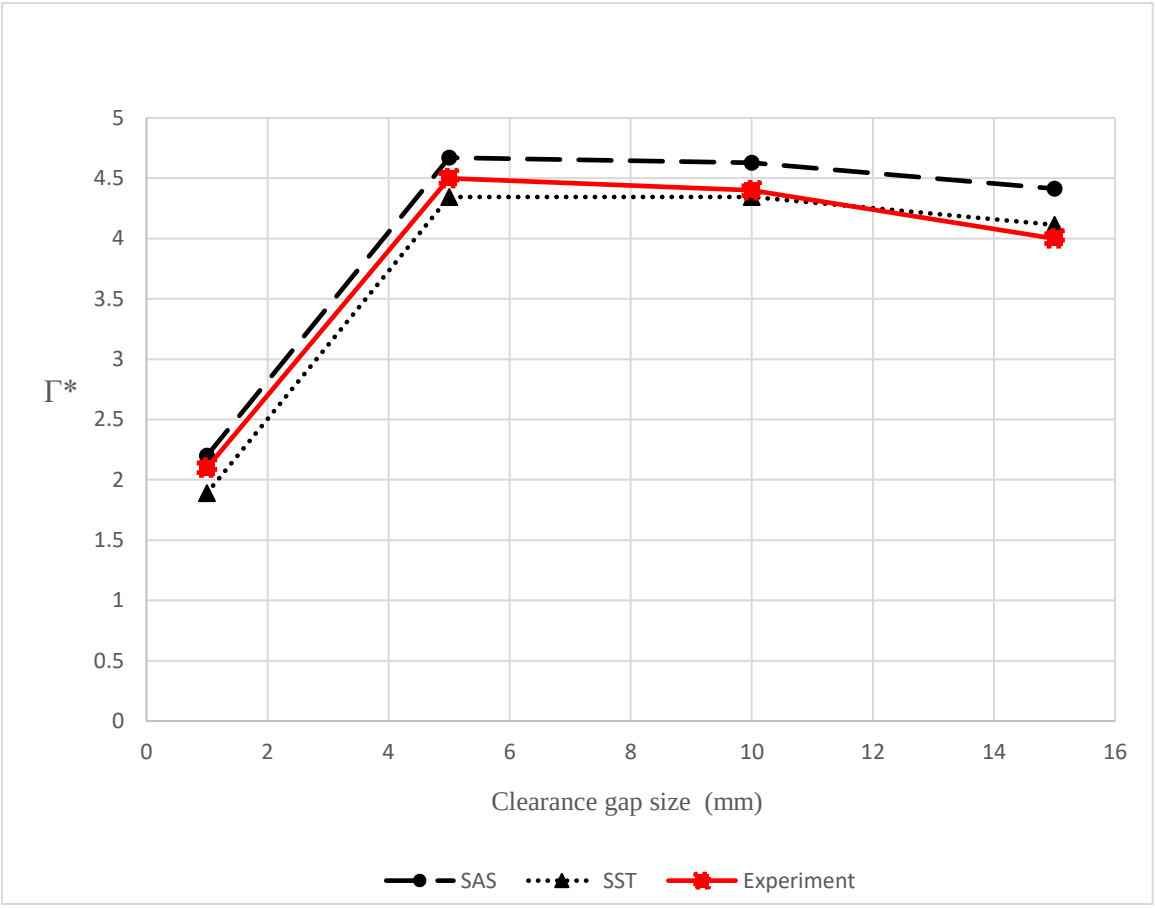

Figure 7. Evolution of non-dimensional circulation strength with different clearance gap sizes. The results are obtained on a plane, perpendicular to the free flow direction, 0.7 chord lengths behind the hydrofoil's trailing edge. Inlet velocity is set to 10m/s with an angle of attack of 7°.

The circulation strength presented in Figure 7, shows a good fit for both the SST and the SAS turbulence models. It is recognized that the SST model has a better fit at the larger clearance gap sizes. Towards the smaller clearance gap sizes it shifts, and SAS model provides a better match than the SST model. As circulation is a global parameter, it could explain the accuracy of the SST model at the larger clearance gap sizes. Smaller clearance gap sizes generate additional unsteadiness, and the SAS model is expected to obtain more accurate results in this area than the SST model. This might be the reason why the SAS model shows better fit for the smaller clearance gap sizes.

Special attention should be given to the points at $1\ mm$ and $10\ mm$ since these clearance gap sizes are used in later simulations. The slope of the curve indicates that the clearance gap of $1\ mm$, is highly dependent on small clearance gap variations, while the $10\ mm$ is only slightly affected by small clearance gap changes.

Figure 8 provides the results of the axial velocity in the vortex core center made dimensionless with the free flow velocity. The minimum pressure defines the vortex core. The normalized axial velocity has a reasonable fit for both models. The SAS model is recognized to have the best fitting shape. Compared with experiment, the SAS model slightly underestimates the larger clearance gap sizes and overestimate the smaller ones.

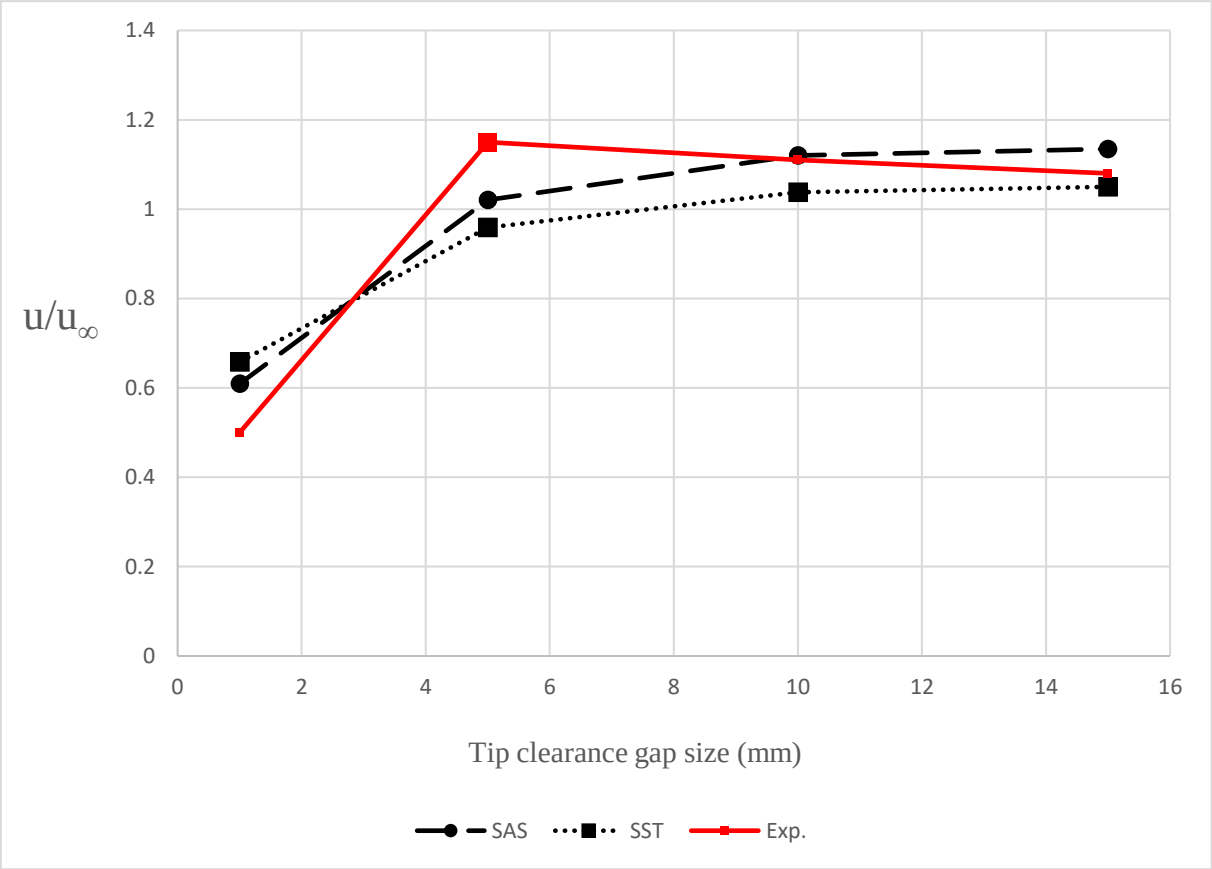

Figure 8. Displayed are the evolution of normalized axial velocities with clearance gap sizes. The results are obtained on a plane, perpendicular to the free flow direction, 0.7 chord lengths behind the hydrofoil's trailing edge. Inlet velocity is set to 10 m/s with an incidence angle of 7°.

Overall there is not much difference between the two turbulence models. This is expected to be a consequence of no separation over the hydrofoil, generating limited global instabilities [31]. For the smaller clearance gap sizes the SAS model provides better results, especially for the axial core velocity. Further simulations will include smaller range of the tip clearance gap sizes. Also, the moving hydrofoil simulation is expected to create flow separations and increased unsteadiness. SAS turbulence model is therefore applied for further simulations.

Lamb-Oseen fit

The vortex model presented in Chapter 3.2 provides an analytical estimation of the vortex behavior. Equation 4 presented in that chapter express how the circulation is distributed from the vortex core. The curves are cropped when the discs surface (Equation 1, Chapter 3.1) intersect with the endwall boundary.

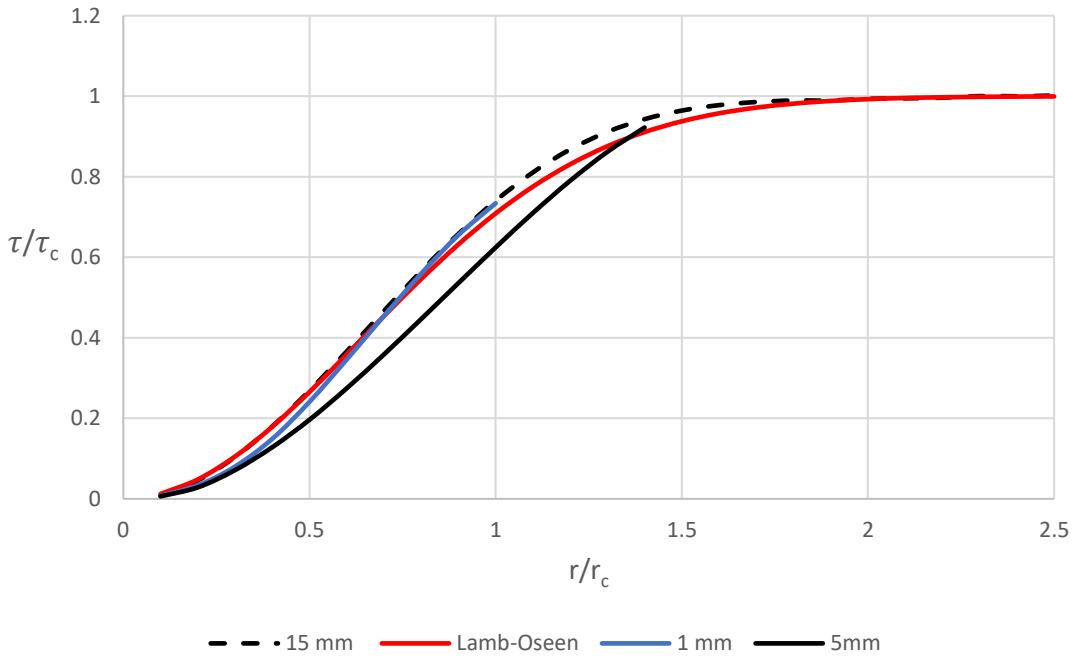

Figure 9 Displayed are the evolution of the circulation strengths by analytical Lamb-Oseen solution and SAS-simulations with the vortex radius. The simulated data is gathered for 10 points per unit on the x-axis. The results are obtained on a plane, perpendicular to the free flow direction, 0.7 chord lengths behind the hydrofoil's trailing edge. Inlet velocity is set to 10m/s with an angle of attack of 7°.

Figure 9 shows three different clearance gap sizes compared to Lamb-Oseen analytical solution for the circulation distribution out of the vortex core center, where the simulated and analytical result has a reasonable agreement. The clearance gap of 1 mm and 10 mm has the best fitted shape compared to the analytical solution. Where the clearance gap of 5 mm has a total circulation deficit at 1 r_c.

5.2 VORTEX MECHANISM

To examine the mechanism of the Tip Leakage Vortex, a flow over a stationary hydrofoil was simulated. Figure 10 presents contour plots of the roll up over the hydrofoil. Figure 11 presents the close up velocity contour for 0.3mm. And Figure 12 presents vortex stabilizing that happen behind the hydrofoil's trailing edge.

The vortex filament over the hydrofoil, showed in Figure 10, provides continuous strength to the TLV from the leading to the trailing edge of the hydrofoil. Figure 10 displays the vorticity (velocity curl) at five different hydrofoil lengths for simulation with stationary hydrofoil and a clearance gap size of 0.3 mm, 1 mm *and* 15 mm for an SAS-SST turbulence model. To make the vortex development clearer, the contour lines for the boundary layers are cropped at the endwall and over the hydrofoil.

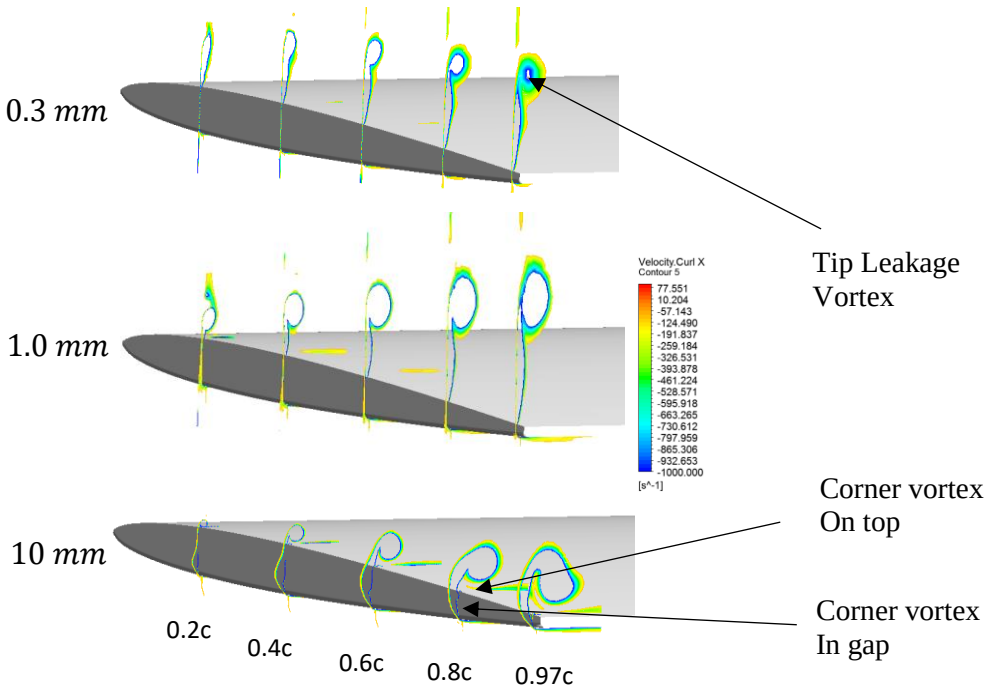

Figure 10. A contour plot describinf the formation of the TLV over the hydrofoil for three different clearance gap sizes ranges. Inlet velocity is set to 10m/s with an angle of attack of 7°.

Due to the pressure difference between suction side and pressure side a leakage jet is created in the clearance gap. Tip corner vortices are recognized as a result of the leakage flow over sharp edges. The corner vortex inside the clearance gap is present for the large gap, but not visual for the small gap, while the Tip Leakage Vortex is created in the area above the hydrofoil. As expected, the formation of the TLV is different between the three clearances. At the larger gap, the corner vortex is merging with Tip Leakage Vortex at the trailing edge. It is observed that there is a more narrow and elliptic vortex shap for the smaller gaps. An explanation to this might be that the small clearance gap prevents flow curvation inside the clearance gap.

For the smallest clearance gap size, 0.3 mm, is it shown in Figure 11 that there is a region with backflow just before the clearance gap. This phenomenon is believed to be a result of the adverse pressure gradient due to the hydrofoil's stagnation point, and the flow's possibility to flow into the clearance gap.

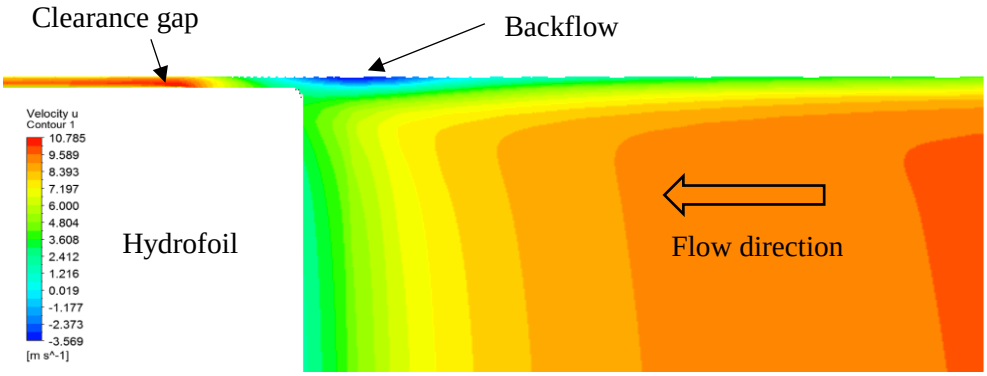

Figure 11. Seen from the above, a plane cutting the hydrofoil streamwise. For the smallest clearance gap size, 0.3mm, there is observed a backflow just before the clearance gap opening.

The thickness of the boundary layer, which seems larger than the clearance gap size, could manage to create a horseshoe vortex (Chapter 3.3), which could explain the backflow.

Figure 12 presents the evolution of the Tip Leakage Vortex from the trailing edge to one chord length behind the hydrofoil for three different clearance gap sizes. The Figure shows the contour plots for five different lengths behind the hydrofoil for three different clearance gap sizes. The leakage flow in the smaller clearance gaps drags on the endwall's boundary layer, creating an induced vortices, seen as the vorticity by the wall at 1 mm and 0.3 mm.

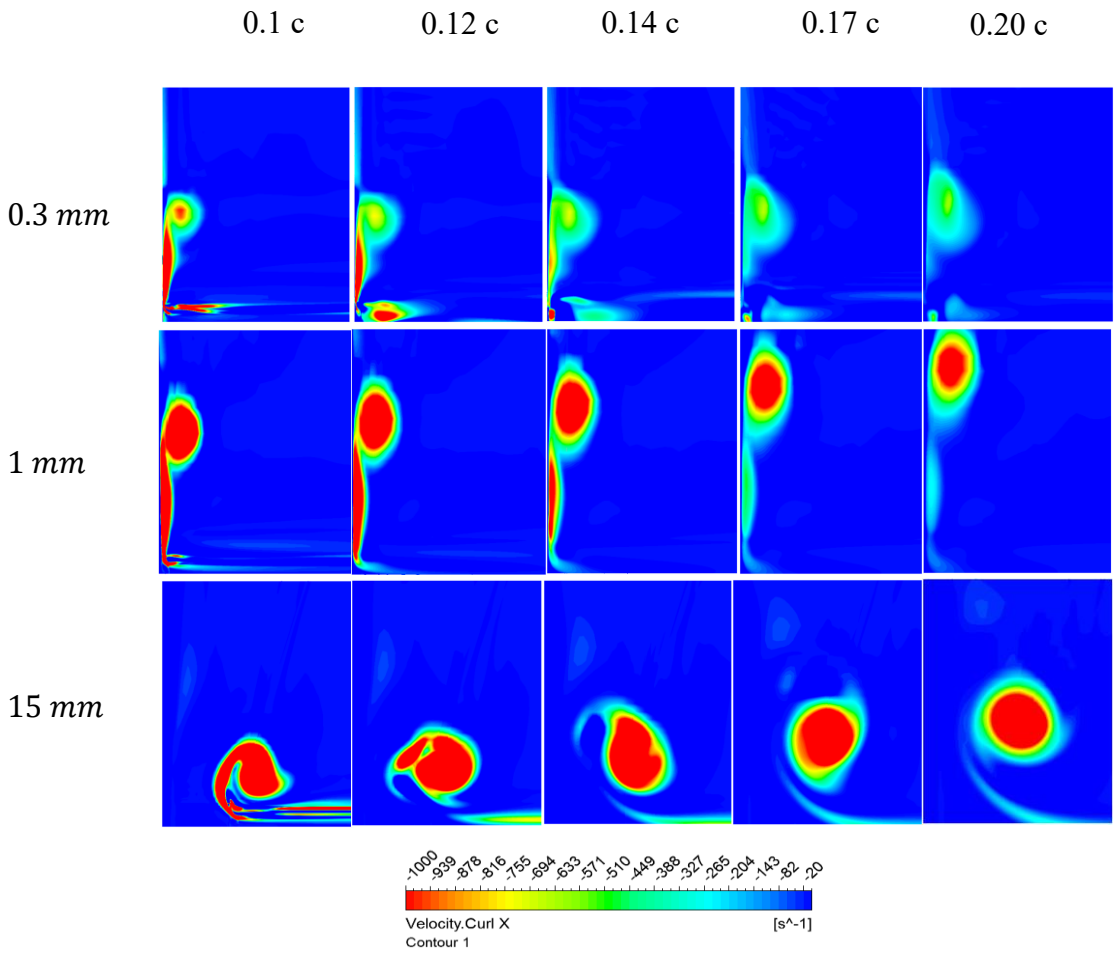

Figure 12. Stabilizing of TLV behind the hydrofoil from trailing edge to 1 chord behind trailing edge. The results are obtained on a plane, perpendicular to the free flow, 0.7 chord lengths behind the hydrofoil's trailing edge. Simulations has applied a SAS-SST turbulence model. Inlet velocity is set to 10m/s with an angle of attack of 7°. c is the chord length.

From Figure 10 and 12, it is recognized that the vortex for a clearance gap of 1.0 mm is the one that deflects most in the upwards direction. It could look like the clearance gap size is working as a nozzle for the leakage flow, where a decreased flow area increases the flow velocity. However, for the smallest clearance gap size, it is considered that the wall effects reduces the strength of the tip flow leakage, and then reduces the upwards deflection for 0.3 mm.

5.3 EFFECTS OF FLUCTUATING THE CLEARANCE GAP SIZE

Presented here is a revised flow model due to the complicity if the results presented in Chapter 5.4/5.5. The aim is to examine the singled out effects of compressing and expanding the clearance gap size. This simplified model has no streamwise velocity, but has included a fluctuating clearance gap. Hence, all flow generated pressure differences are removed. This setup is designed to only catch the overall effects, therefore for accelerated simulations, the mesh densities have been roughened. Figure 13 shows the results for a mean clearance size of 0.3 *mm*, 1.0 *mm, and* 10 *mm* with a displacement of correspondingly 0.03 *mm*, 0.1 *mm*, and 1.0 *mm*.

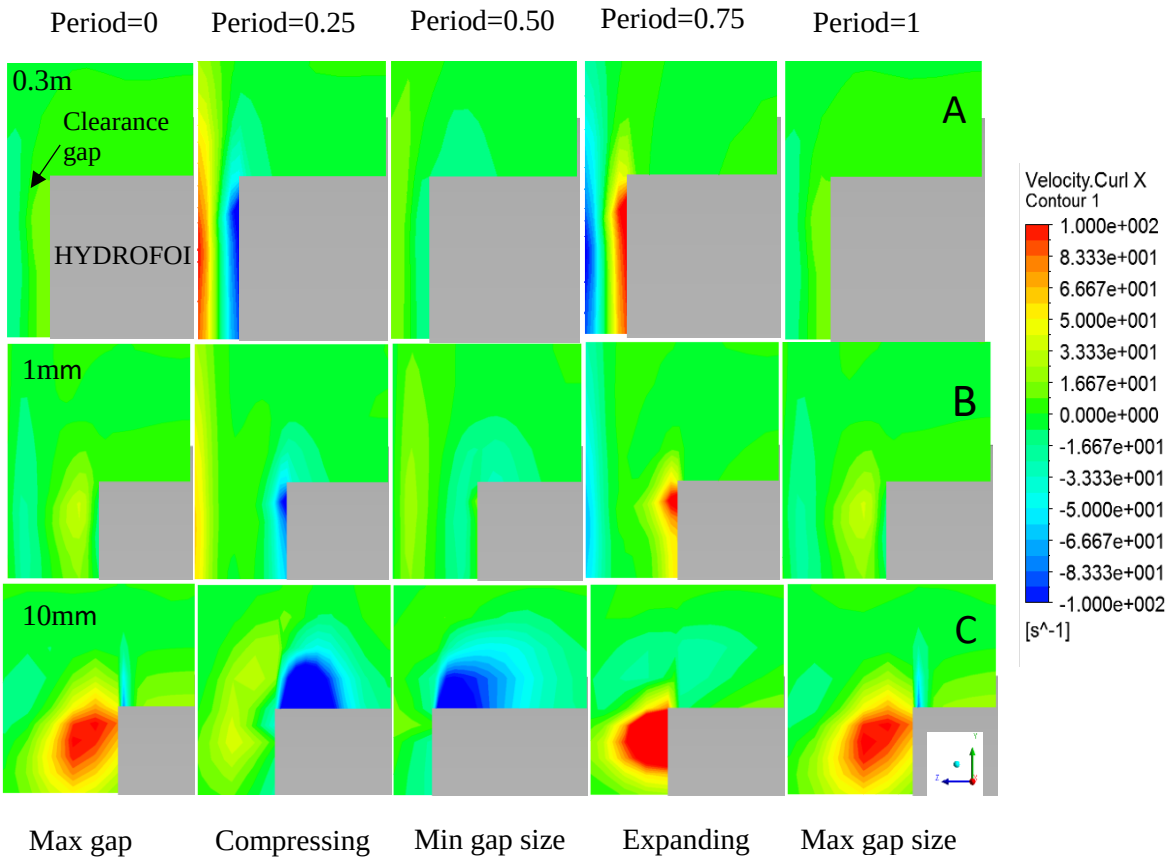

Figure 13. No-flow conditions to avoid flow generated pressure differences. Three different clearance gap sizes, 0.3 *mm,* 1.0 *mm and* 10 *mm, were tested for a fluctuating hydrofoil. Seen is a contour plot of the velocity curl in a range of [-100,100]. The results are obtained on a plane, perpendicular to the "free flow", set on the middle of the hydrofoil.*

The results shown in Figure 13 indicates that the compression and expansion vortices are as expected. For the compression, there is increased pressure in the clearance gap, thus the fluid escapes and rolls over the hydrofoil. The process is reversed for the expansion, generating a vortex that rotates the opposite way. The strongest vortex is observed in the middle of the compression-/expansion-process. This might be a result of the sine wave displacement function (chapter 4.3) that creates a velocity peak in the middle of the compression/expansion.

For the $10\ mm$, it is observed that the compressing vortex is located on the top of the hydrofoil, whereas the expansion vortex is located in the clearance gap size. This could imply that a Tip Leakage Vortex might absorb additional strength for both expansion and compression.

5.4 EFFECTS ON TLV OF FLUCTUATING THE CLEARANCE GAP SIZE

This subchapter presents the results from simulations with a varying clearance gap. The steady state solution was reached. Therefor only one cycle from each simulation is shown. 10 points were needed for capturing a cycle. For every time step, the vortex center is set to where the pressure is minimum. Also, there is minimal stretching of the vortex core. The circulation strengths are therefore calculated over the same surface area (Equation 1, Chapter 3.1) for all time steps.

The frequency of the induced hydrofoil movement is 10 Hz, and the amplitudes are 10 % of the mean clearance gap size. The measuring point was set at the downstream by 0.7 chord lengths, and the selected turbulence model was SAS-SST. Also presented is results from stationary hydrofoil simulations at the maximum and minimum of the fluctuating clearance gap size. The results are presented in the form of non-dimensional circulation strength (Equation 17) over a single fluctuation cycle. Figure 14a-c shows the results for mean clearance gap sizes of respectively 0.3 mm, 1.0 mm and 10 mm. Areas of interest are the fluctuating amplitude and the mean magnitude of the fluctuations compared to stationary cases.

The two smaller gap sizes, Figure 14a (0.3 mm) and 14b (1 mm), show a smooth curve for the circulation strength. The shape of this curve corresponds to the induced displacement function (Chapter 4.3). It can also be seen that the circulation is dependent on the clearance gap size, which is in accordance with earlier results seen in Figure 7 (Chapter 5.1).

From Figure 14b, the clearance gap size of 1 mm is observed to have the same fluctuating amplitude as the difference between the stationary hydrofoils. As realized from Figure 7 (Chapter 5.1), the mean clearance gap of 1 mm is highly affected by small variations of the clearance gap size. This implies that the shape of the curve is a result of the stationary difference in the clearance gap size itself, and not a result of the specific movement of the hydrofoil.

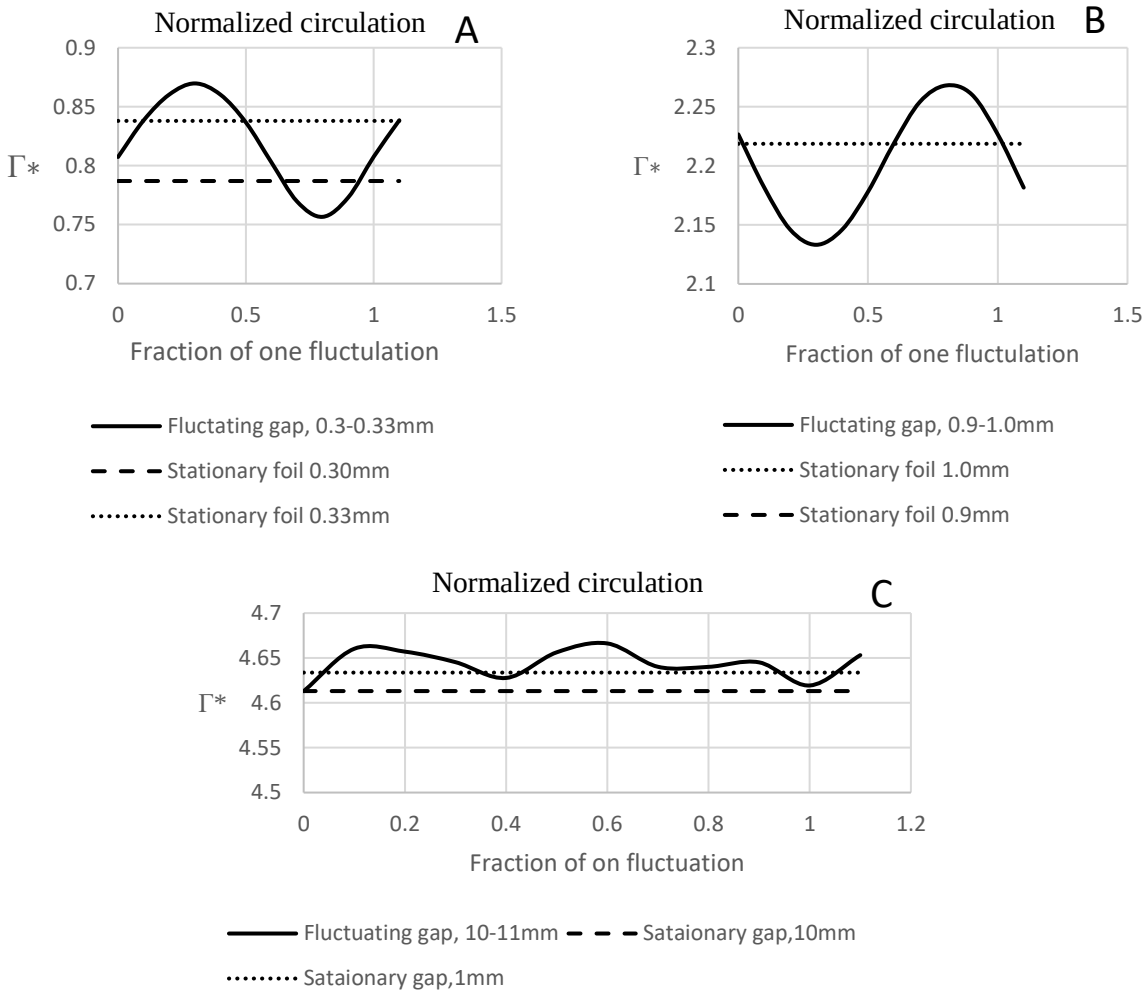

Figure 14. Three different mean clearance gap sizes, a-c, shows the normalized circulation strength reaction with a varying clearance gap size.The results are obtained on a plane, perpendicular to the free flow, 0.7 chord lengths behind the hydrofoil's trailing edge. Simulations have applied an SAS-SST turbulence model. Inlet velocity is set to 10m/s with an angle of attack of 7°.

However, the upwards shift of the curve in Figure 14b could be a result of the specific movement of the hydrofoil. This might indicate that the fluctuating hydrofoil itself create a constant vortex, unaffected by the compression/expansion stadiums. From Figure 13 (Chapter 5.3) it was observed that the compression/expansion generated vortices had slightly different positions, which might play a role.

Overall it looks like the upwards shift of the circulation strength increases with increasing clearance gap size. For the smaller clearance gap sizes, 0.3 mm and 1 mm, the amplitudes of the fluctuations are approximate 5 % of the mean circulation strength. While for the largest clearest gap of 10 mm, the amplitude is approximate 1 %. Thus, the fluctuation has the least

impact on the $10\ mm$ clearance gap. Still, all the amplitudes have the same order of magnitude, and the mean clearance gap size has little affection on the magnitude of the amplitudes.

From Figure 7 (Chapter 5.1), the $10\ mm$ clearance gap indicates an area where circulation strength is limited affected by the clearance gap size. It is therefore naturally that the $10\ mm$ has the smallest amplitude, as seen in Figure 14. Nevertheless, this is contrary to results obtained for the no-flow simulation, Figure 13c (Chapter 5.3), where the largest clearance gap ($10\ mm$) generated the most profound circulation.

As mentioned in the introduction, Tip Leakage Vortex may be subjected to cavitation in the vortex core. The pressure drop is dependent on the vortex circulation strength (Chapter 3.1). Thus, the deviation of the maximum circulation strength is of interest. The maximum circulation strength from the fluctuating clearance gap deviates from the maximum circulation strength from a stationary hydrofoil at around $4\ \%, 2\ \%, \text{and}\ 1\ \%$ for respectively $0.3\ mm, 1.0\ mm$ and $10\ mm$. Whereas the increase in absolute non-dimensional circulation strength values are $0.03, 0.05, and\ 0.032$ correspondingly.

5.5 THE EFFECTS ON THE KAPLAN TURBINE

As mentioned in the introduction, tip leakage might reduce efficiency and create instabilities in the Kaplan turbine. The drag- and lift- forces are two factors that affect the turbine's performance, while the radial force might affect the turbine shaft's wobbling. Presented here are results on how drag, lift, and radial forces are affected by a fluctuating clearance gap sizes. Areas of interest are the fluctuating amplitude and the mean magnitude of the fluctuations compared to stationary cases.

The radial forces with variable clearance gap sizes are shown in Figure 15a-d. Figure 15a presents result for different clearance gap sizes, and 15b-d shows the fluctuating effect for mean clearance gap size of respectively $0.3\ mm$, $1.0\ mm$, and $10\ mm$. Figure 15a presents the radial forces acting on the blade with the clearance gap size. A peak is observed at a clearance gap size of $5\ mm$. This variance of the radial force due to the fluctuation of the clearance gap size might have a stabilizing or destabilizing effect on the turbine shaft's wobbling.

Presented in Figure 15b-d are radial forces with one single fluctuating period for respectively $0.3\ mm$, $1.0\ mm$ and $10\ mm$. The effects are greatest for the smallest ($0.3\ mm$) and the largest ($10\ mm$) clearance gap sizes. The increased values of mean radial force for the fluctuating curve is large, medium and none for correspondingly $0.3\ mm$, $1.0\ mm$ and $10\ mm$. This demonstrates a trend where smaller clearance gaps are more subjected to change from a fluctuating hydrofoil. Nevertheless, the clearance gap size of $10\ mm$ is subjected to severe periodic differences regarding the radial force.

The strong amplitude seen in Figure 15.d ($10\ mm$) could indicate that this clearance gap size is affected by the differences in the compression and expansion stages. This observation is in compliance with the result observed from the no-flow conditions, Figure 13c (Chapter 5.3), where the $10\ mm$ clearance gap provoked the largest velocity curl.

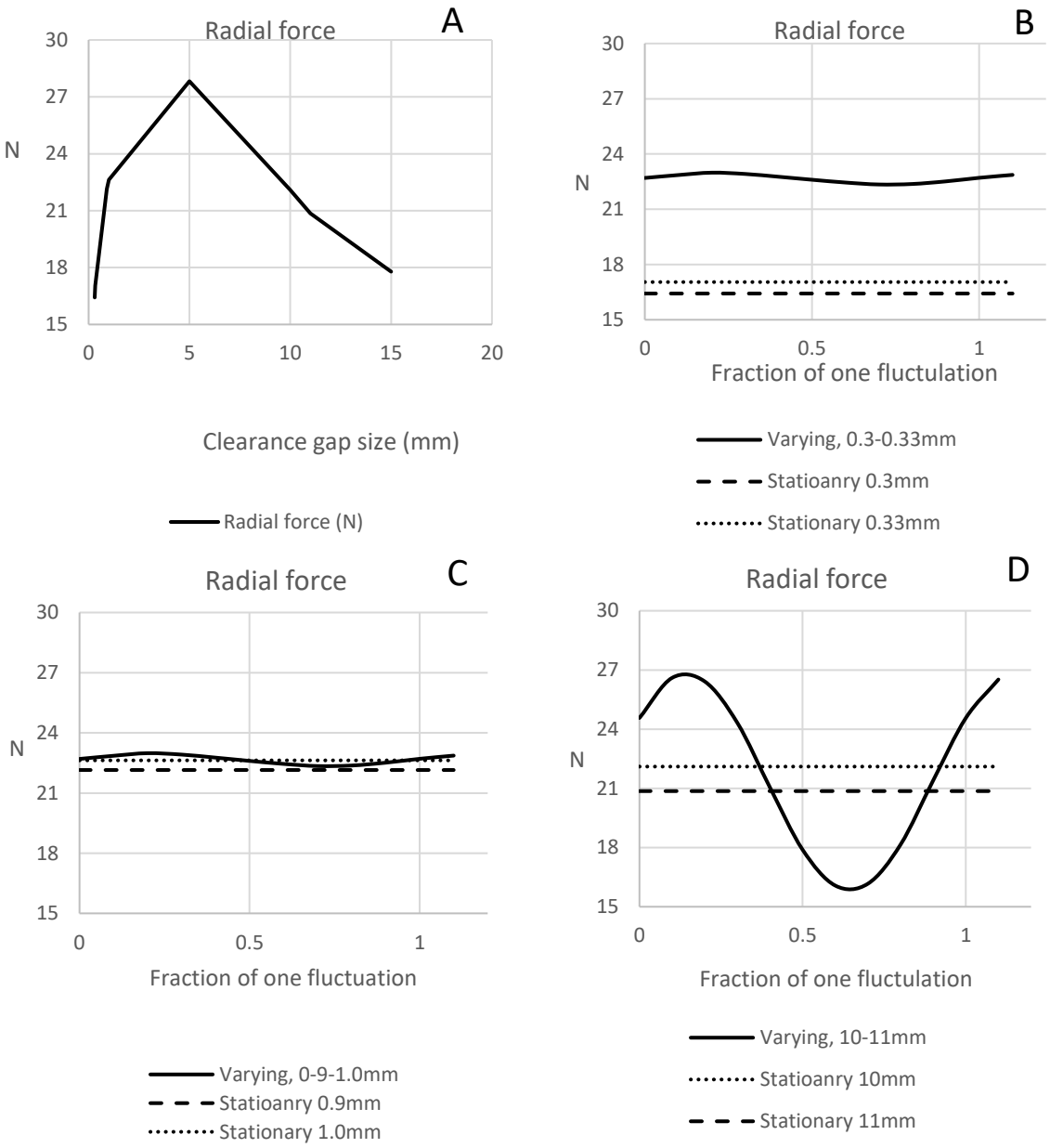

Figure 15. Radial force on the hydrofoil with respect a single fluctuation. Simulations have applied an SAS-SST turbulence model. Inlet velocity is set to 10 m/s with an angle of attack of 7°.

The maximum obtained radial forces in the fluctuations showed rather significant increases compared to the stationary cases. The three test cases, $0.3\ mm$, $1.0\ mm$ and $10\ mm$, showed increases of $36\ \%$, $1.5\ \%$, and $20\ \%$ respectively. Thus, there is no profound trend for these data. However, the values are significant.

Presented in Figure 16 is the lift/drag ratio over a single fluctuation for three different clearance gap sizes, $0.3\ mm$, $1.0\ mm$ and $10\ mm$. The lift/drag ratio is a measure of a hydrofoil's performance, where an increased lift/drag value is a measure of increased hydrofoil performance and vice versa.

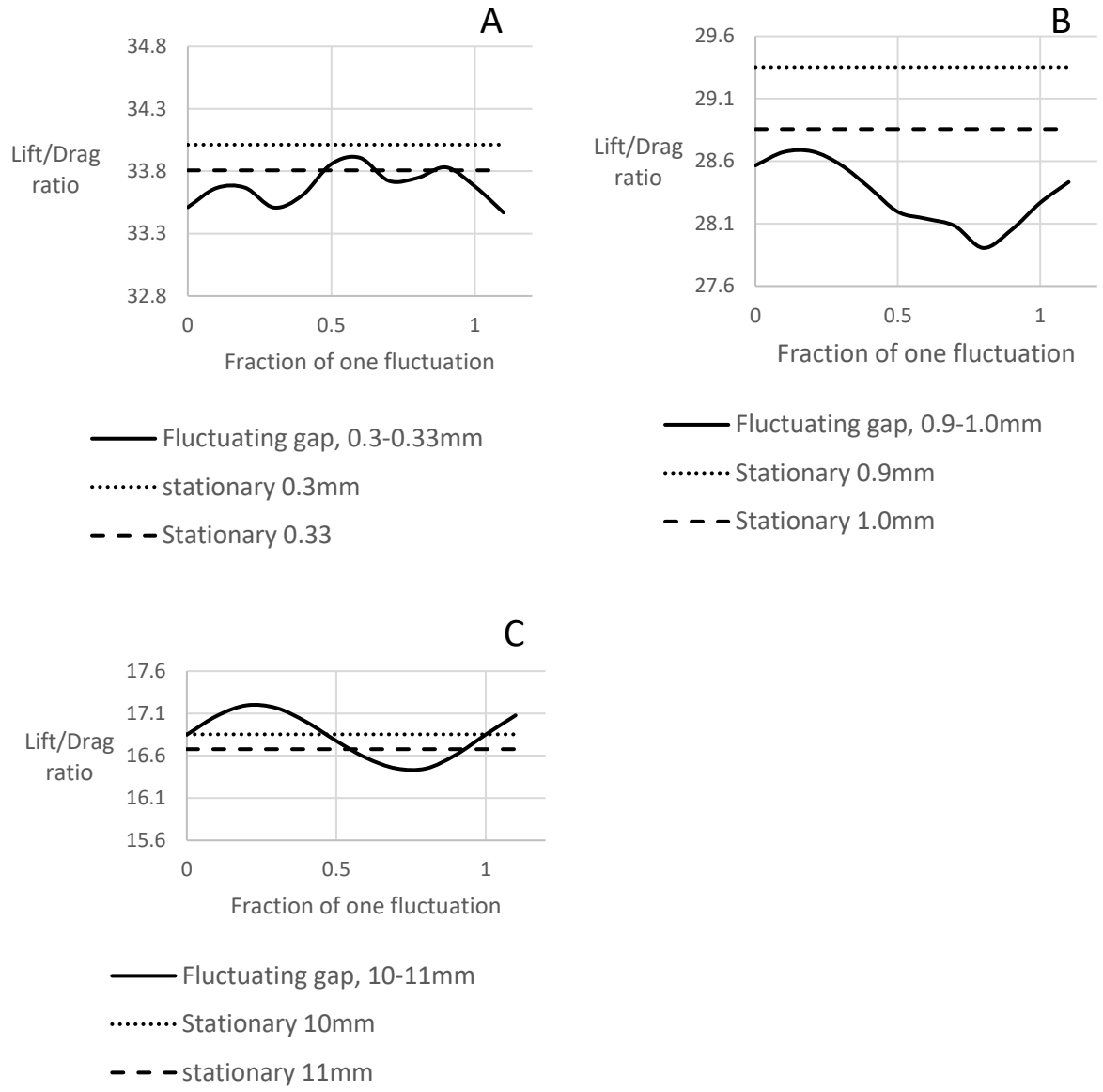

Figure 16. Three different mean clearance gap sizes, a-c, shows how the lift/drag ratio react with a varying clearance gap size. Simulations have applied an SAS-SST turbulence model. Inlet velocity is set to 10 m/s with an angle of attack of 7°.

Registered from Figure 16, for all three mean clearance gap sizes, a fluctuating clearance gap has an overall negative effect on the lift/drag ratio. This observation is most evident for the smallest clearance gaps, while the largest clearance gap, Figure 16c, shows no apparent deviation for the mean lift/drag through a cycle. On the other hand, the largest clearance gap has the biggest amplitude. This demonstrates that the lift/drag ratio might only be dependent on the hydrofoil size, i.e. clearance gap size dependent for this area. The smaller clearance gap sizes, Figure 16b-16c, shows a deficit for lift/drag ratio, but the magnitude of the deficit rather small. The smaller gap sizes reduce the tip leakage and hence increases the lift, but a bigger hydrofoil area also increases the drag. For this case, the increase of the drag force was bigger than the increase of the lift force, which gave a small deficit for the lift/drag ratio.

Figure 16a indicates that the smallest clearance gap size ($0.3\ mm$) struggles to converge to a smooth steady state. This is in contrary to results observed earlier for the circulation strength, seen in Figure 14a, where the graph is smooth. As discussed in Chapter 5.2, a clearance gap size of $0.3\ mm$ is smaller than the endwall's boundary layer thickness, and could thus produce unpredictable values. In this case, a horseshoe vortex might develop and affect the results obtained from the clearance gap of $0.3\ mm$.

6 CONCLUSION

As determined in chapter 2, the effect of a fluctuating clearance gap has been studied, and results show that the effects are not insignificant. The maximum circulation strength was increased for all tested mean clearance gap sizes due to the fluctuating clearance gap. Hence, increasing the risk for cavitation in the vortex core. The clearance gap sizes at $0.3\ mm$, $1.0\ mm$, and $10\ mm$ showed a maximum circulation strength increase of respectively $4\ \%$, $2\ \%$, and $1\ \%$ to the maximum circulation strength observed from the stationary hydrofoils. The trend here is significant, and the fluctuation has more profound fractional effects at smaller clearance gap sizes. The amplitude of the fluctuating curve was largest for the smallest clearance gap sizes, $0.3\ mm$ and $1.0\ mm$, with an amplitude of $5\ \%$ of the mean. Which means that the largest clearance gap size of $10\ mm$ has the most stable TLV. For a stationary hydrofoil, the Tip Leakage Vortex strength reduced drastically with decreasing clearance gap size below $5\ mm$. This also created a nozzle-like reaction, shifting the vortex core location in an upwards direction.

Radial forces and lift/drag ratios were observed for the Kaplan turbine. The radial forces showed a peak for a clearance gap size of $5\ mm$ for the stationary test cases. The effects of fluctuations showed an increase of the maximum radial force of $36\ \%$, $1.5\ \%$, and $20\ \%$ for the clearance gap sizes of respectively $0.3\ mm$, $1.0\ mm$, and $10\ mm$. For this measured parameter, the $1\ mm$ gained the most stable effects. The mean fluctuating lift/drag curve for $0.3\ mm$ and $1.0\ mm$ did deficit correspondingly $0.4\ \%$ and $1.8\ \%$ lower than their minimum lift/drag for a stationary hydrofoil. The fluctuating lift/drag curve for a clearance gap of $10\ mm$ showed no mean deviation, but the amplitude reached $\pm\ 4\ \%$ of mean lift/drag value.

Simulated results validated against experimental showed a slightly better fit for the SAS-SST turbulence model compared to the SST turbulence model. As more turbulence might was generated in gap for the smaller clearance gap sizes, the SAS-SST model provided better results. Where for the larger clearance gap sizes with less turbulence, the SST-model was slightly better for the circulation strength.

The single out fluctuation effects were observed for simulations without any induced flow. Simulated results showed that the compression and expansion of the clearance gap size created different rotating vortices, where the $10\ mm$ clearance gap size achieved largest vortices with shifting locations.

A backflow was observed for the smallest clearance gap size of $0.3\ mm$. This might be a negative consequence of a smaller clearance gap size than the endwall's boundary layer thickness. However, when the clearance gap is as small as $0.3\ mm$, wall casing treatment might provide positive effects. As described in Chapter 2.1, wall casing treatment has obtained effective results at relatively small clearance gap sizes [20-22].

The overall energy production from the Kaplan turbine is affected by the Tip Leakage Vortex, including erosion from cavitation and efficiency loss. Simulations display that these negative effects worsened when including wobbling from the turbine shaft, resulting in a decreased lift/drag ratio and an increased vortex strength. Since hydropower is such a big part of the world's electricity production, negligible small efficiency changes could have a significant impact on the larger picture. Hence, it is important to chase after improvements in the hydropower industry. Hopefully, this thesis' observation could motivate for further research.

7 FURTHER WORK

The aim of this thesis is to investigate potential research gaps in the Tip Leakage Vortex (TLV) field. Based on the findings, a new niche area has been identified. In this thesis, the niche area has only been marginally researched. Hence, for industrial applicable results, further investigation is needed.

The observed effects on the TLV caused by the shaft wobbling were for the most negative. Ways to stabilize the turbine is therefor of interest. As the wobbling remains, minimization of the negative effects are desirable. It is therefore necessary to examine the effects with altering parameter values of the clearance gap size, blade pressure differences (incidence angle, wing profile), Reynolds number, the frequency of the fluctuations, an amplitude of fluctuations, and blade diameter.

The identified niche area has not yet been researched experimentally. Experimental data is important for validating the numerical models. It could be necessary for future investigations to include experiments.

8 REFERENCES

1. MCCABE, G. *Snow and horseshoe vortices*. 2012 [cited 2017 27.05]; Available from: http://mccabism.blogspot.no/2012/02/snow-and-horseshoe-vortices.html.
2. Zhou, C. and H. Hodson, *The tip leakage flow of an unshrouded high pressure turbine blade with tip cooling.* Journal of Turbomachinery, 2011. **133**(4): p. 041028.
3. Holstad, M. *Elektrisitet*. 2016 30. November. 2016 [cited 2017 05.06]; Available from: https://www.ssb.no/energi-og-industri/statistikker/elektrisitet/aar.
4. Council, W.E. *Energy resources: Hydropower*. 2016 [cited 2017 02.05.2017]; Available from: https://www.worldenergy.org/data/resources/resource/hydropower/.
5. Kjersti Aarrestad, L.M.H., *ENERGY AND WATER RESOURCES IN NORWAY.* Norwegian ministry of petroleum and energy, 2015.
6. Lakshminarayana, B., M. Pouagare, and R. Davino, *Three-Dimensional Flow Field in the Tip Region of a Compressor Rotor Passage—Part I: Mean Velocity Profiles and Annulus Wall Boundary Layer.* Journal of Engineering for Power, 1982. **104**(4): p. 760-771.
7. Lakshminarayana, B. and A. Ravindranath, *Interaction of compressor rotor blade wake with wall boundary layer/vortex in the end-wall region.* Journal of Engineering for Power, 1982. **104**(2): p. 467-478.
8. Lakshminarayana, B. and A. Pandya, *Tip clearance flow in a compressor rotor passage at design and off-design conditions.* Journal of engineering for gas turbines and power, 1984. **106**(3): p. 570-577.
9. DREYER, M., *Mind The gap: tip leakage vortex dynamics and cavitation in axial turbines*. 2015, ÉCOLE POLYTECHNIQUE FÉDÉRALE DE LAUSANNE.
10. Wu, S., et al. *Influence of blade tip rounding on tip leakage vortex cavitation of axial flow pump*. in *IOP Conference Series: Materials Science and Engineering*. 2013. IOP Publishing.
11. Miorini, R.L., H. Wu, and J. Katz, *The internal structure of the tip leakage vortex within the rotor of an axial waterjet pump.* Journal of Turbomachinery, 2012. **134**(3): p. 031018.
12. You, D., et al., *Effects of tip-gap size on the tip-leakage flow in a turbomachinery cascade.* Physics of Fluids, 2006. **18**(10): p. 105102.
13. Decaix, J., et al., *RANS and LES computations of the tip-leakage vortex for different gap widths.* Journal of Turbulence, 2015. **16**(4): p. 309-341.

14. Higashi, S., Y. Yoshida, and Y. Tsujimoto, *Tip leakage vortex cavitation from the tip clearance of a single hydrofoil.* JSME International Journal Series B Fluids and Thermal Engineering, 2002. **45**(3): p. 662-671.
15. Zhao, H., et al., *Numerical investigations on tip leakage flow characteristics and vortex trajectory prediction model in centrifugal compressor.* Proceedings of the Institution of Mechanical Engineers, Part A: Journal of Power and Energy, 2016. **230**(8): p. 757-772.
16. Lampart, P., *Tip leakage flows in turbines.* TASK Quart, 2006. **10**(2): p. 135-175.
17. Muthanna, C. and W.J. Devenport, *Wake of a compressor cascade with tip gap, part 1: Mean flow and turbulence structure.* AIAA journal, 2004. **42**(11): p. 2320-2331.
18. Wang, Y. and W.J. Devenport, *Wake of a compressor cascade with tip gap, part 2: effects of endwall motion.* AIAA journal, 2004. **42**(11): p. 2332-2340.
19. Ma, R., *Unsteady turbulence interaction in a tip leakage flow downstream of a simulated axial compressor rotor*. 2003, Virginia Tech.
20. Legras, G., N. Gourdain, and I. Trebinjac, *Numerical analysis of the tip leakage flow field in a transonic axial compressor with circumferential casing treatment.* Journal of Thermal Science, 2010. **19**(3): p. 198-205.
21. Qiang, X.-Q., M.-M. Zhu, and J.-F. Teng, *Effect of circumferential grooves casing treatment on tip leakage flow and loss in a transonic mixed-flow compressor.* Journal of Theoretical and Applied Mechanics, 2013. **51**(4): p. 903-913.
22. Motycak, L., A. Skotak, and R. Kupcik. *Kaplan turbine tip vortex cavitation–analysis and prevention*. in *IOP Conference Series: Earth and Environmental Science*. 2012. IOP Publishing.
23. Li, W., et al., *Numerical simulation of active control on tip leakage flow in axial turbine.* Chinese Journal of Aeronautics, 2009. **22**(2): p. 129-137.
24. Behr, T., *Control of rotor tip leakage and secondary flow by casing air injection in unshrouded axial turbines*. 2007, Dresden University of Technology, Germany.
25. Mulu, B., et al., *Simulation-based investigation of unsteady flow in near-hub region of a Kaplan Turbine with experimental comparison.* Engineering Applications of Computational Fluid Mechanics, 2015. **9**(1): p. 139-156.
26. Cervantes, M., U. Andersson, and H. Lövgren. *Turbine-99 unsteady simulations–Validation*. in *IOP Conference Series: Earth and Environmental Science*. 2010. IOP Publishing.

27. Javadi, A. and H. Nilsson. *Unsteady numerical simulation of the flow in the U9 Kaplan turbine model*. in *IOP Conference Series: Earth and Environmental Science*. 2014. IOP Publishing.
28. Cercantes, M., V. Fredriksen, Editor. 2017.
29. Tryggeson, H., *Analytical Vortex Solutions to the Navier-Stokes Equation (doktorsavhandling)*. 2007, ISBN.
30. Holmén, V., *Methods for vortex identification.* Master's Theses in Mathematical Sciences, 2012.
31. ANSYS, I., *ANSYS CFD-Post User's Guide*. 2013.
32. Baker, C., *The laminar horseshoe vortex.* Journal of fluid mechanics, 1979. **95**(02): p. 347-367.
33. Cengel, Y.A., J.M. Cimbala, and M. Kanoğlu, *Fluid mechanics, fundamentals and applications, 2011*. McGraw Hill, New York.
34. ANSYS, I., *ANSYS CFX-Solver Theory Guide*. 2013.
35. Kuron, M. *3 Criteria for Assessing CFD Convergence* 2015 [cited 2017.
36. Saad, T. *TURBULENCE MODELING FOR BEGINNERS*
37. Schmitt, F.G., *About Boussinesq's turbulent viscosity hypothesis: historical remarks and a direct evaluation of its validity.* Comptes Rendus Mécanique, 2007. **335**(9-10): p. 617-627.
38. Alfonsi, G., *Reynolds-averaged navier–stokes equations for turbulence modeling.* Applied Mechanics Reviews, 2009. **62**(4): p. 040802.
39. Menter, F.R., *Two-equation eddy-viscosity turbulence models for engineering applications.* AIAA journal, 1994. **32**(8): p. 1598-1605.
40. Davidson, L. *Evaluation of the SST-SAS model: channel flow, asymmetric diffuser and axi-symmetric hill*. in *ECCOMAS CFD 2006: Proceedings of the European Conference on Computational Fluid Dynamics, Egmond aan Zee, The Netherlands, September 5-8, 2006*. 2006. Delft University of Technology; European Community on Computational Methods in Applied Sciences (ECCOMAS).
41. Celik, I.B., U. Ghia, and P.J. Roache, *Procedure for estimation and reporting of uncertainty due to discretization in {CFD} applications.* Journal of fluids {Engineering-Transactions} of the {ASME}, 2008. **130**(7).

APPENDIX

N-S CYLINDER

$$\frac{\partial v_r}{\partial t} + v_r\frac{\partial v_r}{\partial r} + v_z\frac{\partial v_r}{\partial z} - \frac{v_\theta^2}{r} = -\frac{1}{\rho}\frac{\partial p}{\partial r} + v(\nabla^2 v_r - \frac{v_r}{r^2})$$

$$\frac{\partial v_\theta}{\partial t} + v_r\frac{\partial v_\theta}{\partial r} + v_z\frac{\partial v_\theta}{\partial z} + \frac{v_\theta v_r}{r} = v(\nabla^2 v_\theta - \frac{v_\theta}{r^2}) \quad (17)$$

$$\frac{\partial v_z}{\partial t} + v_r\frac{\partial v_z}{\partial r} + v_z\frac{\partial v_z}{\partial z} = -\frac{1}{\rho}\frac{\partial p}{\partial z} + v\nabla^2 v_z$$

MESH INDEPENDENCE STUDY

	$Parameter$	$Elements$	$Drag\ (N)$	$Lift\ (N)$	$v_\theta\ (m/s)$	$Axial\ core\ velocity\ (m/s)$
$Fine$	M_1	16400444	24.41	405.45	4.12	10.96
$Medium$	M_2	7250368	24.56	405.17	4.09	10.90
$Coarse$	M_3	3608680	25.01	404.25	3.94	10.71
	R_{21}	1.296	1.30	1.30	1.30	1.30
	R_{32}	1.285	1.29	1.29	1.29	1.29
	e_{21}		0.15	-0.28	-0.03	-0.06
	e_{32}		0.45	-0.92	-0.15	-0.19
	P		4.32	4.61	5.73	4.79
	r^P		3.07	3.30	4.41	3.47
	M_{ext}^{21}		24.34	405.57	4.13	10.98
	M_{ext}^{32}		24.34	405.62	4.16	11.00
	e_a^{21}		0.006	0.001	0.008	0.005
	e_a^{32}		0.018	0.002	0.036	0.018
	e_{ext}^{21}		0.003	0.000	0.002	0.002
	e_{ext}^{32}		0.009	0.001	0.017	0.008
	GCI_{fine}^{21}		0.36 %	0.04 %	0.30 %	0.26 %
	GCI_{medium}^{32}		1.10 %	0.12 %	1.32 %	0.90 %

FFT: VORTEX SHREDDING

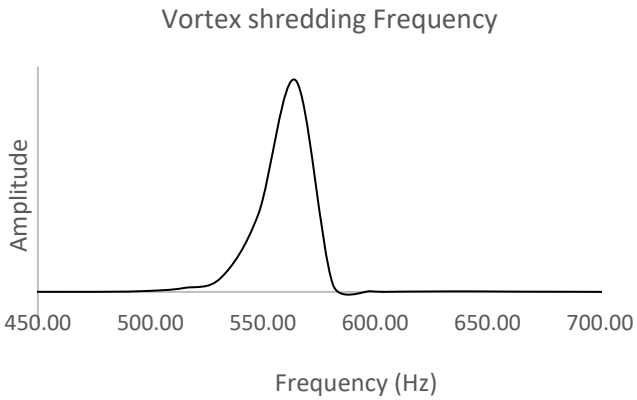

NEPAL CONFERENCE PAPER

Proceedings of the International Symposium on Current Research in Hydraulic Turbines

CRHT – VII

April 04, 2017, Turbine Testing Lab, Kathmandu University, Dhulikhel, Nepal

Paper no. _ _ _

Numerical investigation of tip leakage vortex

Vegard Fredriksen[1]

[1]Department Energy and Process Engineering, Norwegian University of Science and Technology, Alfred Getz veg 4, 7491 Trondheim, Norway

Corresponding author (vegaf@stud.ntnu.no)

Abstract

In axial rotating machinery, a clearance gap between blade tip and casing is present, allowing a flow leakage, and resulting in a tip leakage vortex (TLV) downstream of the machinery. This could lead to unwanted effects like cavitation and flow instabilities. This paper numerically investigates effects from varying tip rounding and tip clearance gap size at steady state conditions with SST turbulence model.

Keywords: Tip leakage vortex, tip rounding, clearance gap, steady, SST

1. INTRODUCTION

Axial rotating machinery, i.e. Kaplan turbines, needs small clearance gap between the blade tip and casing to allow the blades to rotate freely. In the clearance gap, pressures difference over the turbine blade drives a tip leakage flow, which eventually shreds over to a Tip Leakage Vortex (TLV). Resulting in a lowered pressure in vortex core that might lead to cavitation. This phenomenon has been widely covered but is not yet fully understood. This paper will numerically give an insight into the mechanisms around TLV and will be validated with an experiment done by M. Dreyer [1]. The area around controlling TLV will be further investigated.

The importance of controlling the TLV has motivated many researchers. Wall casing treatment has experimentally been researched by Dreyer [1], Ma[2] and numerically by Legras et al. [3] and Qiang et al. [4], obtaining a reduced tip leakage flow at no penalty to the performance. Still, wall casing treatment has yet only sufficient results at unreal small clearance gap sizes. Another method, anti-cavitation lip, a small "wall" on the pressure side of the blade, has been studied by Dreyer [1] and Motycak [5], obtaining result of shifting the vortex core without affecting the turbine efficiency. Another method, described by Behr [6], blade tip injection, needs further investigation. This paper will focus on two other important controlling factors, blade tip rounding, covered by Wu [7], and tip clearance gap size, described in detail by Dreyer [1], Wu [7], You [8], Decaixa [9] and Higashi [10]. With plenty of research in the area, there are still unknown effects, like transient clearance gap size effects, which the author will cover in his master thesis. Whereas this paper will provide pre-research including steady state numerical investigation of blade tip rounding- and tip clearance gap size effects.

2. METHODOLOGY

2.1 Computational setup

To match experimental results obtained by Dreyer [1], a NACA0009 wing profile, originally 110mm, here truncated at 100mm, with maximum height $h = 9.9$, is used with an uniform inlet velocity at 10 m/s and incidence angle at 7°. This simplified scaled model of a Kaplan turbine blade, placed in a 150x150mm tunnel, is computed at one chord length upstream and five chord lengths downstream, given a total tunnel length of seven chord lengths. The simulations was conducted at steady state with a high-resolution numerical scheme and SST turbulence model with an iteration stop at residual RMS of 10^{-5}. Ansys' softwares ICEM meshing and CFX solver was used.

A new dimensionless variable is introduced for evaluating the effects of the clearance size.

$$\tau = \frac{Tip\ clearance\ gap}{h} \tag{1}$$

2.2 Mesh analysis

To evaluate the numerical convergence three different mesh densities were tested at steady state with SST turbulence, using the procedure described by Celik [11]:

$$p = \frac{1}{\ln(r)} |\ln|\frac{\epsilon_{32}}{\epsilon_{21}}|| \tag{2}$$

Where $r = 1.4$, $\epsilon_{21} = \Phi_2 - \Phi_1, \Phi_k\ is\ solution\ on\ k^{th}\ mesh$

$$\Phi_{ext}^{21} = \frac{r^p \Phi_1 - \Phi_2}{r^p - 1} \tag{3}$$

$$e_a^{21} = |\frac{\Phi_1 - \Phi_2}{\Phi_1}| \tag{4}$$

$$GCI_{fine}^{21} = \frac{1.25 e_a^{21}}{r^p - 1} \tag{5}$$

Mesh independence test was executed on a sharp edged tip geometry with mesh densities 13.7, 5.2 and 1.9 million hexahedral elements with a constant mesh refinement factor of 1.4. Applying the above produce yields results shown in table 1. The deviation between medium and fine mesh shows converging characteristics, especially for the axial core velocity and eddy dissipation. It is observable that the order of accuracy is locally defined. Tangential velocity, v_θ, shows some deviation between the medium and fine mesh.

Table 1: Result from Grid Convergence Index analysis

	$V_{\theta,\max}$ (m/s)	**Force x** (N)	**Axial core velocity** (m/s)	**Turbulent eddy dissipation** Area average ($m^2 s^3$)
Φ_1 (fine)	3.91	25.45	10.01	13.48
Φ_2 (Medium)	3.69	26.02	9.75	13.31
Φ_3 (Coarse)	3.18	26.93	7.83	12.47
r	1.40	1.40	1.40	1.40
e21	-0.22	0.57	-0.26	-0.17
e32	-0.51	0.91	-1.92	-0.84
P	2.57	1.39	5.94	4.75
r^p	2.37	1.60	7.38	4.94
$\Phi_{ext.}^{21}$	4.06	24.50	10.05	13.52
ea21	0.06	0.02	0.03	0.01
ea32	0.14	0.03	0.20	0.06
e21.ext	0.04	0.04	0.00	0.00
e32.ext	0.09	0.06	0.03	0.02
GCI21	5 %	5 %	1 %	0 %
GCI32	13 %	7 %	4 %	2 %

For steady state simulations, the fine mesh will be used at different clearance gap sizes and for the rounded blade tip. The hexahedral mesh was constructed in ICEM.

The mesh structure, as shown in figure 1, show a sectional mid chord the foil of the fine mesh with a curved edge at pressure side.

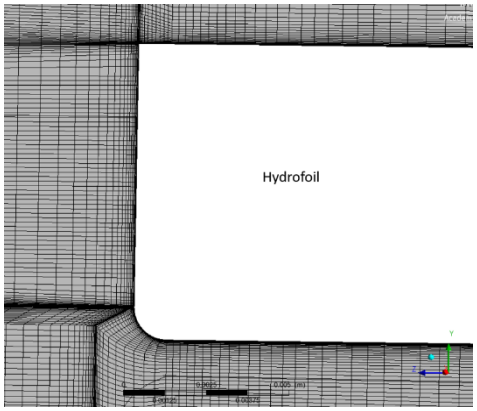

Figure 1: Mid chord mesh sectional

3. RESULT AND DISCUSSION

Flow configuration used is the same as for the mesh analysis with an uniform inlet velocity of 10 m/s, angle of attack of 7°, simulating a flow over the descried NACA0009 wing profile at steady state.

3.1. Experimental comparison

The circulation Γ is calculated by Lamb-Oseen Vortex model:

$$v_\theta(r) = \frac{\Gamma}{2\pi r}(1 - e^{-\frac{ar^2}{r_c^2}}) \tag{6}$$

Where $a \approx 1{,}25643$, the tangential velocity v_θ, the critical radius r_c and the radius r.

The normalized circulation is describes as:

$$\Gamma^* = \frac{\Gamma}{w_\infty * r_c} \tag{7}$$

Where w_∞ is the freestream velocity.

The plots, Figure 2 and 3, shows the effects on respectively Circulation and Axial velocity when changing the tip clearance gap size. The data is measured 0.7 chord lengths behind the tailing edge of the foil. The experimental result is gathered from Dreyer [1].

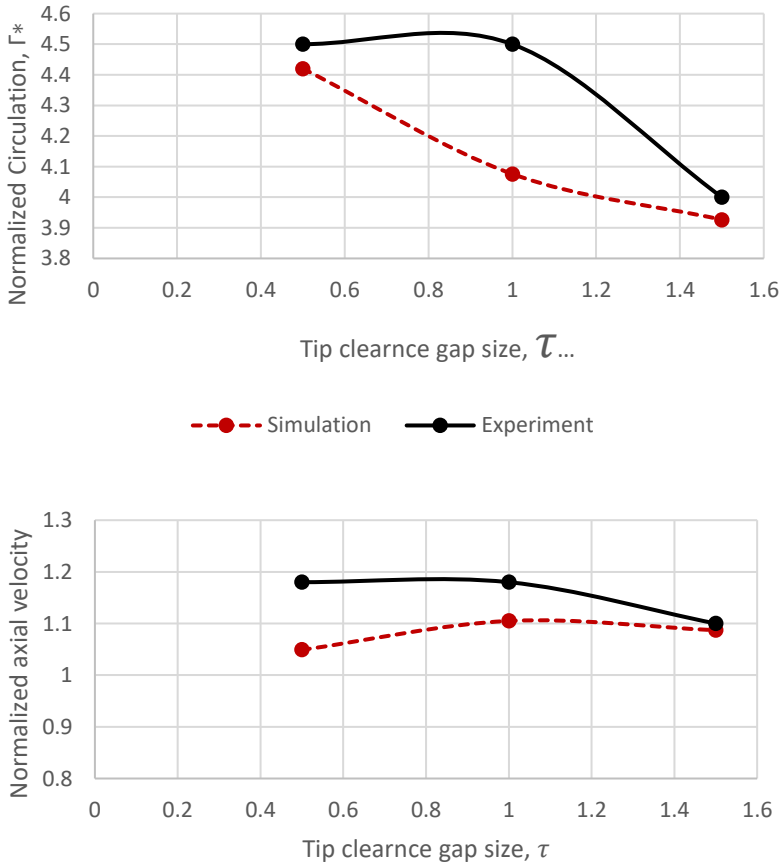

Figure 2 and 3: Simualted and experimental comaparison of tip clearnace gap size effects

The comparison in Figure 2 and 3 shows that the simulations result are somewhat correct. There could be many reasons of the deviations, but the simulated results are valid to use. An interesting observation is that the TLV circulation strength is decreasing with increasing clearance gap for calculated points.

Tip clearance gap size effects could be observed in Figure 4, obtaining a velocity contour plot of the TLV 0.7 chord lengths downstream the foil's trailing edge. Figure 4 indicates that the location of the vortex core is highly affected by the tip clearance size. Thus, there is possibilities to shift the vortex core away from critical areas. Accurate estimations of the TLV trajectory remains yet to be established.

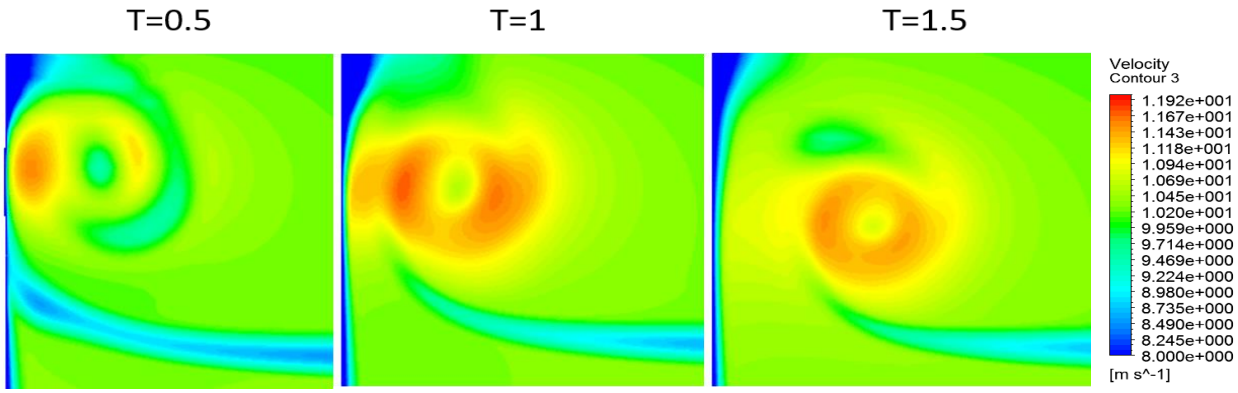

Figure 4: Contour plot of absolute velocity 0.7 chord lengths downstream of trailing edge.

3.2 The vortex behavior

The vortex behavior is obtained by plotting the tangential velocity out from the vortex center, seen in figure 5. The vortex is observed at 0.7 chord lengths behind the hydrofoil's trailing edge. The vortex core acts like a rigid body, while the outer region has an irrational behavior.

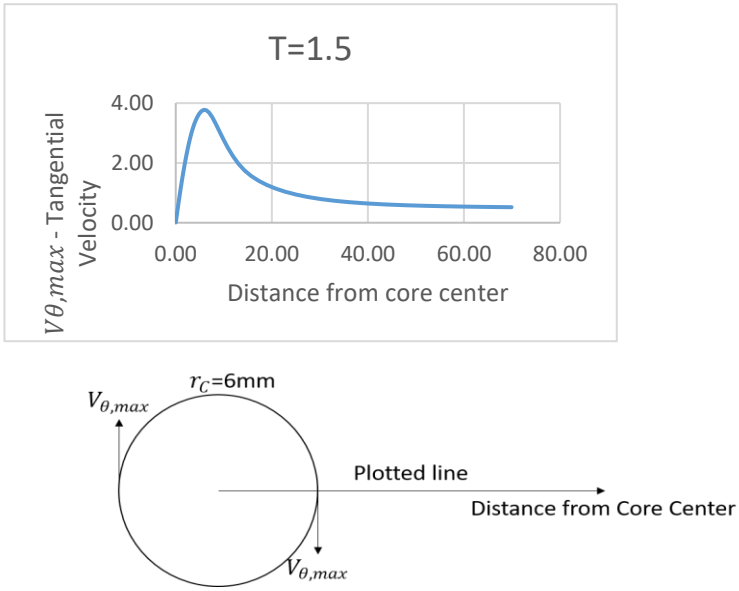

Figure 5: Plotted tangteial velocity in radial direction from vortex

3.3 Tip rounding effects

Two different tip geometries were tested, one sharp tipped, and one with a curved edge of radius 1mm at a clearance size of $\tau = 1.5$. The contour plot, Figure 6, shows the vorticity generated at three different chord lengths over the hydrofoil. As expected, the tip separation vortex, point A, is higher for the sharp tip. While point B shows the formation of the TLV. This is in accordance with results obtained by Wu [7]. By adding a small edge curve, the corner vortex is reduced. As shown by Wu [7], with an increasing tip rounding, the corner vortex (A) disappears.

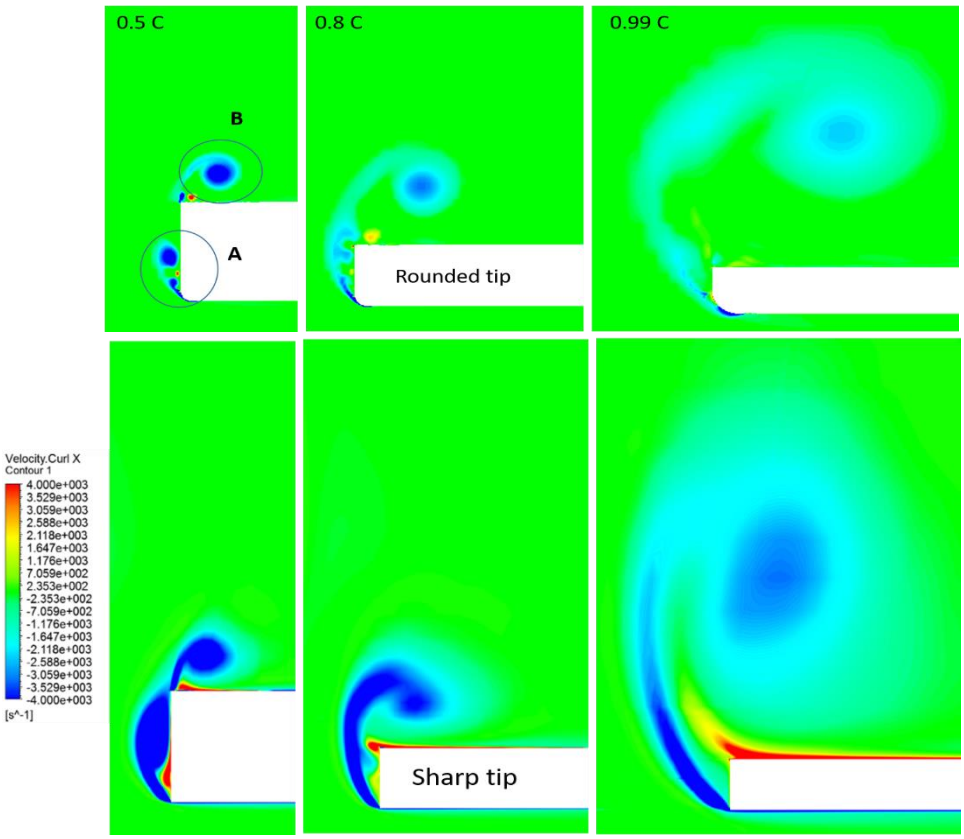

Figure 6: Vortex formation for rounded and sharp tip at three different chord locations

Wu [7] states that an increased rounding of the tip will increase the tip leakage flow and thus also the downstream TLV. While Dreyer [1] obtained experimental result that showed identical TLV for both cases. Obtained simulation results, figure 7, shows a contour plot of the vorticity 0.7 chord lengths downstream the foil's tailing edge, indicating a somewhat stronger effects on the rounded tip.

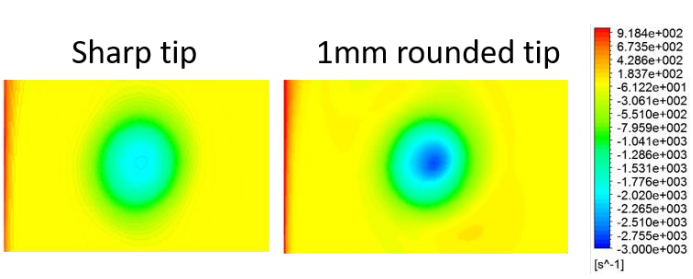

Figure 7: TLV strength of sharp and rounded tip

9 CONCLUSION

Both tip clearance gap size and tip rounding affect the mechanism and strength of the Tip Leakage Vortex. The rounded tip yield a stronger vortex strength than the sharp tip. While there is not found any optimal tip clearance gap size regarding the vortex strength, thus, this area still need further investigation.

10 FURTHER WORK

The author will continue the work on TLV. Interesting results for different clearance gaps motivates for further investigation within this area. This paper is limited to steady state simulation. The author will continue the work and apply a transient clearance gap size.

11 REFERENCES

1. Dreyer, M., Mind The Gap: Tip Leakage Vortex, 2015, DREYER, M., "Mind The gap: tip leakage vortex dynamics and cavitation in axial turbines". Diss. ÉCOLE POLYTECHNIQUE FÉDÉRALE DE LAUSANNE, 2015.
2. Ma, R., "Unsteady Turbulence Interaction in a Tip Leakage Flow Downstream of a Simulated Axial Compressor Rotor", Diss. Virginia Tech, 2003.
3. Legras, Guillaume, N. Gourdain, and Isabelle Trebinjac. "Numerical analysis of the tip leakage flow field in a transonic axial compressor with circumferential casing treatment." Journal of Thermal Science 19.3 (2010): 198-205.
4. Qiang, X.; Zhu, M.; Teng, T., "Effect of circumferential grooves casing treatment on tip leakage flow and loss in a transonic mixed-flow compressor." Journal of Theoretical and Applied Mechanics 51.4 (2013): 903-913.
5. Motycak, L.; Skotak, A.; Kupcik, R., "Kaplan turbine tip vortex cavitation–analysis and prevention." IOP Conference Series: Earth and Environmental Science. Vol. 15. No. 3. IOP Publishing, 2012.
6. Behr, T., "Control of rotor tip leakage and secondary flow by casing air injection in unshrouded axial turbines. Diss. Dresden University of Technology", Germany, 2007
7. Wu, S.; Shi, W.; Zhang, D., "Influence of blade tip rounding on tip leakage vortex cavitation of axial flow pump. OP Conference Series: Materials Science and Engineering", Vol. 52. No. 6. IOP Publishing, 2013.
8. You, D. Wang, M; Moin, P.; Mittal, R., "Effects of tip-gap size on the tip-leakage flow in a turbomachinery cascade", Physics of Fluids 18.10 (2006): 105102.
9. Decaixa, J, "RANS and LES computations of the tip-leakage vortex for different gap widths", 2014, Journal Of Turbulence (ISSN: 1468-5248), vol. 16, num. 4, p. 309-341
10. Higashi, S., "Tip Leakage Vortex Cavitation from the Tip Clearance of a Single Hydrofoil", In: CAV 2001: Fourth International Symposium on Cavitation, June 20-23, 2001, California Institute of Technology, Pasadena, CA USA2
11. Celik, I.B.; Ghia, U.; Roache, P.J.; Freitas, C.J. "Procedure for estimation and reporting of uncertainty due to discretization in CFD applications" ASME J. Fluids Eng. 2008, 130.

NTNU HSE	Hazardous activity identification process	Prepared by HSE section Approved by The Rector	Number HMSRV2601E	Date 09.01.2013 Replaces 01.12.2006

Unit: *EPT* **Date: 07.06.2017**

Line manager:

Participants in the identification process (including their function)**:**

Short description of the main activity/main process: Master project for student Vegard Fredriksen.
Project title: Numerical investigation of tip leakage vortex

Is the project work purely theoretical? YES: *Answer "YES" implies that supervisor is assured that no activities requiring risk assessment are involved in the work. If YES, briefly describe the activities below. The risk assessment form need not be filled out.*

Signatures: *Michel Cervantes:* *Vegard Fredriksen:* Vegard

ID nr.	Activity/process	Responsible person	Existing documentation	Existing safety measures	Laws, regulations etc.	Comment
	Numerical simulations	Vegard Fredriksen				